

Magnetic Fields, Star Formation Rates and Gas Densities at Sub-kpc Scales in a Pilot Sample of Nearby Galaxies

SOUVIK MANNA¹ AND SUBHASHIS ROY¹

¹*National Center for Radio Astrophysics, TIFR,
Pune University Campus, Ganeshkhind, Pune 411007, India*

ABSTRACT

We have estimated the magnetic field strengths of a sample of seven galaxies using their non-thermal synchrotron radio emission at metre wavelengths, and assuming energy equipartition between magnetic fields and cosmic ray particles. We tested for deviation of magnetic fields from energy equipartition with cosmic ray particles, and found that deviations of $\sim 25\%$ are typical for the sample galaxies. Spatially resolved star formation rates (SFR) were estimated for the seven galaxies along with five galaxies studied previously. For the combined sample of twelve galaxies, the equipartition magnetic fields (B_{eq}) are correlated with the SFR surface densities (Σ_{SFR}) at sub-kpc scales with $B_{\text{eq}} \propto \Sigma_{\text{SFR}}^{0.31 \pm 0.06}$, consistent with model predictions. We estimated gas densities (ρ_{gas}) for a sub-sample of seven galaxies using archival observations of the carbon monoxide (CO) rotational transitions and the atomic hydrogen (HI) 21 cm line and studied the spatially-resolved correlation between the magnetic fields and ρ_{gas} . Magnetic fields and gas densities are found to be correlated at sub-kpc scale as $B_{\text{eq}} \propto \rho_{\text{gas}}^{0.40 \pm 0.09}$. This is broadly consistent with models, which typically predict $B \propto \rho_{\text{gas}}^{0.5}$.

Keywords: Radio continuum emission — Interstellar medium — Star formation — Magnetic fields

1. INTRODUCTION

Magnetic fields are believed to influence several physical processes in a galaxy at almost every scale (e.g. Elmegreen 1981; Niklas & Beck 1997; Groves et al. 2003; Price & Bate 2008; Adebahr et al. 2013). Magnetic fields have been found to consist of two main components: a small-scale turbulent magnetic field up to a few hundred parsecs (e.g. Batchelor 1950; Groves et al. 2003) and a large-scale “ordered” or “regular” magnetic field component at scales of a few kpcs (e.g. Moss & Shukurov 1996; Shukurov et al. 2006; Kulsrud & Zweibel 2008). Magnetic fields in galaxies can be measured using their effects on different radiation processes like Zeeman splitting of emission lines, polarized emission from dust, the polarization of starlight, Faraday rotation of polarized radio emission, and intensity of synchrotron emission which we use in this work. Measurement of the line-of-sight component of the magnetic field via the Zeeman effect in galaxies other than the Milky Way has been possible for only a few systems (Kazes et al. 1991; Sarma et al. 2005; Robishaw et al. 2008); a significant expansion of such studies is very difficult with current-generation telescopes.

Magnetic fields in galaxies can be measured and studied using synchrotron emission at radio frequencies, at scales larger than the resolution of the radio observation. For example, a Very Large Array (VLA) polarization study of NGC 4736 at 8.46 and 4.86 GHz found that the magnetic field in the galaxy was ordered in a spiral shape (Chyży & Buta 2008). An X-shaped structure of the magnetic field in the galactic halo region was observed by stacking the Karl G. Jansky VLA polarized emission maps of 16 nearly edge-on spiral galaxies, obtained as part of the CHANG-ES survey (Krause et al. 2020); such structures had also been observed in individual spiral galaxies (e.g. Krause et al. 2006; Krause 2009; Heesen et al. 2009). However, polarized radio emission from external individual galaxies is difficult to study at low radio frequencies due to Faraday depolarization (e.g. Sokoloff et al. 1998).

The average magnetic field strength can also be estimated from the total intensity of synchrotron radio emission, assuming energy equipartition between magnetic fields and cosmic ray particles (e.g. Miley 1980; Beck & Krause 2005). Equipartition magnetic fields have been studied in several nearby galaxies, but primarily at frequencies >1 GHz (e.g. Chyży et al. 2000; Soida et al. 2001; Heesen et al. 2009; Fletcher et al. 2011; Adebahr et al. 2013). Vargas et al. (2018) studied a sample of three nearby edge-on galaxies from the CHANG-ES survey to separate the thermal Bremsstrahlung from the non-thermal synchrotron emission at 1.5 and 6 GHz. At these frequencies, the thermal component is large and hence the correction for the thermal emission can be as large as $\sim 20\%$, making the derived magnetic field strengths prone to errors. Conversely, the steep spectral index of synchrotron emission implies that it will dominate the total emission at frequencies < 1 GHz, with $\sim 95\%$ contribution (Basu et al. 2012b; Roy & Manna 2021). Thus, magnetic field strengths derived using observations at <1 GHz are very robust to any correction for thermal emission.

Magnetic fields are believed to play an important role at various stages of the star-formation process - from the fragmentation of clouds at the few kpc scales to the final collapse of gas into stars (e.g. Elmegreen 1981; Crutcher 1999; Price & Bate 2008; Van Loo et al. 2015). To understand the influence of magnetic fields and star-formation activities on different physical processes in the ISM at different physical scales, several studies on radio-infrared correlations have been carried out in the past (e.g. Murphy et al. 2006a,b, 2008; Tabatabaei et al. 2013). Magnetic fields (B) and star formation rate surface densities (SFRSD) are expected to be correlated (Niklas & Beck 1997). Semi-analytical model also predicts a strong correlation between B and SFRSDs (Σ_{SFR}) as $B \propto \Sigma_{\text{SFR}}^{1/3}$ at sub-kpc scales to explain the local radio-FIR correlation (Schleicher & Beck 2013, 2016). Observational studies of the correlation between B and star formation rates (SFR) have been done primarily in samples of nearby dwarf galaxies. For example, Chyży et al. (2011) studied 12 local group dwarf galaxies to find that the galaxy-averaged magnetic field and the SFR follow $B \sim \text{SFR}^{0.30 \pm 0.04}$, consistent with the prediction of $B \propto \Sigma_{\text{SFR}}^{1/3}$. However, Jurusik et al. (2014) found the same power-law index in a sample of Magellanic type dwarf galaxies to be 0.25 ± 0.02 , somewhat lower than the expectation. Recently, a study of the dwarf galaxy IC 10 by Basu et al. (2017) provides the only study of the correlation between spatially-resolved magnetic fields and SFRSDs; these authors found that the SFRSD is related to the magnetic field as $B \propto \Sigma_{\text{SFR}}^{0.35 \pm 0.03}$. Therefore, it is important to test such predictions by carrying out systematic spatially-resolved studies of magnetic fields in galaxies and their connection to the star formation rate in nearby large galaxies.

The energy density of magnetic fields and gas in galaxies are expected to be in equipartition, which implies $B \propto \sqrt{\rho_{\text{gas}}}$ (e.g. Chandrasekhar & Fermi 1953; Groves et al. 2003). The observed Radio-FIR correlation can be explained based on such equipartition between the energy density of magnetic fields and gas (Niklas & Beck 1997). Several other numerical magnetohydrodynamic (MHD) simulations of the ISM have predicted the coupling constant (k) between magnetic fields and gas ($B \propto \rho_{\text{gas}}^k$) to be in the range of $\approx 0.4-0.6$ (Fiedler & Mouschovias 1993; Kim et al. 2001; Thompson et al. 2006). Niklas & Beck (1997) studied the correlation between galaxy-integrated equipartition magnetic fields and gas densities for a sample of 43 galaxies to find a power-law index of 0.48 ± 0.05 ; the observed correlation is consistent with $B \propto \sqrt{\rho_{\text{gas}}}$. Although the correlation between gas surface densities and SFRSDs has been extensively studied in the nearby Universe (Kennicutt-Schmidt law; e.g. Kennicutt 1998a; Onodera et al. 2010; Roychowdhury et al. 2015), systematic studies of spatially-resolved correlations between magnetic fields, SFRs and gas densities in nearby galaxies are yet to be carried out. It is thus important to carry out a systematic investigation of both the B- ρ and the B-SFR correlations, at high-spatial resolutions (\approx sub-kpc scales), using direct estimates of the magnetic fields, gas densities, and star-formation rates, in a sample of nearby galaxies. In this paper, we present a pilot study of the connection between spatially resolved magnetic fields, SFRSDs and gas densities in a sample of nearby galaxies.

We have selected a sample of 46 galaxies (Sample 0; Table 2) from the Spitzer Local Volume Legacy (LVL) sample of 258 galaxies within 11 Mpc (Dale et al. 2009). As a pilot project, seven (Sample 1; Table 2) of these 46 galaxies have been observed with the Giant Metrewave Radio Telescope (GMRT) at 0.33 GHz (Roy & Manna 2021). Six of our seven sample galaxies are spirals and the other one is a dwarf irregular Magellanic-type galaxy.

In this paper, we present spatially resolved equipartition magnetic field (B_{eq}) maps of the seven galaxies in Sample 1 (Table 2). We also incorporate the magnetic field maps of five galaxies studied by Basu et al. (2012a) from previous GMRT observations in our study. We derived SFRSD maps of all 12 galaxies (Sample 2; Table 2) using extinction-free diagnostics and used these maps to study the relation between SFRSDs and B_{eq} at sub-kpc scales in our pilot study. We used available archival CO and HI 21 cm data to measure the gas densities (ρ_{gas}) of seven (Sample 3; Table 2) of the combined sample of 12 galaxies and studied the correlation between ρ_{gas} and B_{eq} in these galaxies. We also studied the magnetic field-gas connection through an indirect measurement of their coupling coefficient using radio-FIR correlations of the galaxies in Sample 1.

Table 1. Details of the seven sample galaxies. Note that the images at 0.33 GHz were obtained from observations with the GMRT reported in Roy & Manna (2021) while those at 1.4 GHz were obtained from archival VLA data. The distances to the galaxies were taken from Dale et al. (2009). Galaxies with an asterisk are those for which spatially-resolved CO data are available.

Name	Class	Distance (Mpc)	Inclination angle (deg)	Position angle (deg)	uv range (k λ)	Angular resolution (arcsec ²)	Spatial resolution (pc)	RMS (0.33 GHz) (μ Jy/beam)	RMS (1.4 GHz) (μ Jy/beam)	VLA Project ID (1.4 GHz)
NGC 2683	Sb	7.7	83	43	0.19 - 15	19 \times 13	670	200	40	AI23
NGC 3627*	SAB	10.	65	170	0.26 - 25	16 \times 11	760	800	370	AS541, AP462
NGC 4096	SABc	8.3	76	20	0.14 - 17	14 \times 12	730	100	25	16A-013
NGC 4449	Irregular	4.2	0	0	0.15 - 15	26 \times 15	360	300	180	AB167
NGC 4490	SBm	8.0	60	126	0.13 - 14	19 \times 18	560	230	100	AA181
NGC 4826*	SAab	7.5	60	120	0.22 - 20	15 \times 14	650	280	70	AS541
NGC 5194*	Sbc	8.0	20	10	0.15 - 10	23 \times 18	740	310	30	AB505, AN57

Table 2. List of different samples studied in this paper.

Sample Name	Galaxies
Sample 0	Full sample containing 46 galaxies from Spitzer LVL survey
Sample 1	Pilot sample containing 7 galaxies from Sample 0; galaxies listed in Table 1
Sample 2	Sample 1 + 5 galaxies (NGC 1097, NGC 4736, NGC 5055, NGC 5236 and NGC 6946) from Basu et al. (2012b) = 12 galaxies; used to probe the B_{eq} -SFRSD correlations
Sample 3	A subset of 7 galaxies (NGC 3627, NGC 4826, NGC 5194, NGC 4736, NGC 5055, NGC 5236 and NGC 6946) from Sample 2 which have archival CO data; used to study the B_{eq} -gas density correlations

The paper is organized as follows. The analysis of the data is discussed in Section 2. In Section 3, we present the results of our analysis, including the correlation between magnetic fields, SFRSDs and gas densities of the seven galaxies in Sample 1. In Section 4, we have extended our study to include a sample of five galaxies of Basu et al. (2012a). We discuss the results in Section 5. A summary of this paper is presented in Section 6.

2. DATA ANALYSIS

As can be seen in Table 1, six of the seven galaxies in Sample 1 are spirals of varying inclination angles. The seventh galaxy NGC 4449 is a dwarf irregular galaxy. Basic information about the seven sample galaxies, including their types, distances, inclination angles, position angles, angular resolutions, spatial resolutions, and RMS noise obtained on the GMRT and VLA images are also listed in Table 1. The distances, inclination angles, and position angles of the galaxies were taken from Dale et al. (2009). Radio observations and the data reduction procedures are discussed in detail in Roy & Manna (2021). Briefly, we used GMRT 0.33 GHz observations (covering 0.309–0.342 GHz) and archival VLA observations at 1.4 and \sim 6 GHz to derive non-thermal emission maps for each galaxy. We used H α and 24 μ m observations of the seven galaxies to model free-free emission from them and subsequently, we subtracted the modelled free-free emission from the observed radio emission to get the non-thermal radio maps at 0.33, 1.4 and \sim 6 GHz (Roy & Manna 2021). To generate the non-thermal spectral index maps, we used the non-thermal radio maps at 0.33 and \sim 6 GHz for NGC 2683, NGC 3627, NGC 4096, and NGC 4449. For the rest of the galaxies (NGC 4490, NGC 4826, and NGC 5194), we used non-thermal images at 0.33 and 1.4 GHz to generate the non-thermal spectral index maps (Roy & Manna 2021). In the following subsections, we present the analysis of other ancillary data and relevant measurements.

2.1. Magnetic Field Strengths

The average magnetic field strengths can be estimated from the observed synchrotron flux densities, assuming energy equipartition between cosmic ray particles and magnetic fields (“Classical Equipartition Formula”, e.g. Pacholczyk 1970; Miley 1980; Longair 2011). The equipartition condition is achieved when the total energy in magnetic fields and cosmic ray particles is minimum.

The classical equipartition formalism has shortcomings that lead to an overestimation of the magnetic field strength (B) at regions of steep spectral indices and underestimation of B at flat spectral index regions. To overcome these shortcomings of the classical equipartition formula, Beck & Krause (2005) proposed a revised formula to estimate the average magnetic field strength. The formula is expressed as

$$B_{\text{eq}} = [4\pi(K_0 + 1)E_p^{1-2\alpha_{nt}} \frac{f(\alpha_{nt}) I_\nu \nu^{\alpha_{nt}}}{C_4(i) l}]^{\frac{1}{\alpha_{nt}+3}} \quad (1)$$

K_0 , E_p , I_ν , and α_{nt} are the number density ratio of cosmic ray protons to electrons, the proton rest mass energy, the intensity of the synchrotron emission at frequency ν , and the spectral index of synchrotron emission, respectively. $f(\alpha_{nt})$ is a function of α_{nt} given as $f(\alpha_{nt}) = (2\alpha_{nt} + 1)[2(\alpha_{nt} - 1)c_2(\alpha_{nt})c_1^{\alpha_{nt}}]$ (Beck & Krause 2005). $C_4(i)$ is a constant that depends on the inclination angle (i) of the galaxy and is expressed as $C_4(i) = [\cos(i)]^{(\gamma+1)/2}$, where $\gamma = (2\alpha_{nt} + 1)$. l is the path length of the synchrotron emission. The path length was assumed to be 1 kpc for a galaxy with an inclination angle of 0 degree (face-on). For galaxies with low- and moderate- inclination angles ($< 75^\circ$), the assumed path length was corrected for the inclinations of the galaxies as $l/\cos(i)$. For the two nearly edge-on galaxies in Sample 1, NGC 2683 and NGC 4096, we have assumed an oblate spheroidal shape of the synchrotron emission, such that the diameter on the plane of the galaxy is equal to its major axis. The path lengths (l) were then appropriately calculated, with the path length being maximum (equal to the galaxy's major axis) at the optical centre of the galaxy and gradually declining to the edge of the galaxy. We note that B_{eq} has only a weak dependence on l as $B_{\text{eq}}(r) = l(r)^{\frac{-1}{\alpha_{nt}+3}}$ and hence is less sensitive to the exact choice of l . Values of K_0 and E_p were assumed to be 100 and 938.28 MeV, respectively, the same as used by Beck & Krause (2005). Finally, we used non-thermal radio maps at 0.33 GHz (I_ν) and spectral index maps (α_{nt}) made using 0.33 and 1.4 or ~ 6 GHz radio observations (Roy & Manna 2021) to produce magnetic field maps of the sample galaxies using Equation 1.

The revised equipartition formula diverges for spectral index values ≤ 0.5 because such flat spectra indicate energy loss of electrons through ionizations or Coulomb interactions (Sarazin 1999). The central bulge and arm regions have a mostly flatter spectrum due to the association of star-forming regions and the estimates of equipartition magnetic fields in such regions might be affected by systematic uncertainties. This issue affects the derived magnetic field strengths for 8%, 12%, 3%, 70%, 17%, 7%, and 6% of the projected total surface area of NGC 2683, NGC 3627, NGC 4096, NGC 4449, NGC 4490, NGC 4826, and NGC 5194, respectively. We note that a large fraction of the derived magnetic field values are affected for NGC 4449 due to its non-thermal spectral indices being predominantly flat. This could bias the B_{eq} for NGC 4449.

2.1.1. Uncertainties on Magnetic Field Maps

The procedure we used to estimate the uncertainties on our magnetic field maps is similar to that of Basu & Roy (2013). We used a Monte Carlo method that generated 10^4 random flux density values for each pixel in a galaxy map at 0.33 GHz and either 1.4 GHz or 6 GHz. These flux density values have Gaussian probability distributions with rms values equal to the measured rms of each of the 0.33 and 1.4/6 GHz maps. For each of the 10^4 intensity maps, we computed a magnetic field map using the procedure described in the beginning of Section 2.1. The rms of these 10^4 magnetic field maps provided us with the magnetic field uncertainty maps for each of the seven galaxies in sample 1.

2.2. Star Formation Rates

Rest frame $\text{H}\alpha$ and ultraviolet (UV) observations are the best tracers of recent SFRs as the radiation from these predominantly originate in newly formed massive stars. However, the observations are affected by extinction caused by interstellar dust in both the host galaxy as well as the Milky Way. SFRs estimated from $\text{H}\alpha$ and UV observations are therefore corrected for the extinction. Dust-corrected SFRs can be estimated by combining far-ultraviolet (FUV) and $\text{H}\alpha$ data with infrared (IR) data to exploit the complementary strengths at different wavelengths (e.g. Kennicutt & Evans 2012a; Buat 1992; Meurer et al. 1995, 1999; Cortese et al. 2008; Leroy et al. 2012). In addition to the FUV+IR and $\text{H}\alpha$ +IR tracers, the low-frequency radio emission from galaxies, which is predominantly optically thin synchrotron emission, can be used to estimate their dust-unobscured SFRs via the radio-FIR correlation (e.g. Yun et al. 2001).

We estimated the spatially-resolved star formation rates of our Sample 1 galaxies using FUV+ $24\mu\text{m}$, $\text{H}\alpha$ + $24\mu\text{m}$, and 1.4 GHz data, which are discussed, respectively, in the following Sections, 2.2.1, 2.2.2, and 2.2.3. We used data of these different frequencies as tracers in order to (1) get a fair comparison between different SFR diagnostics and (2) for studying star-formation history at different timescales. All SFRs in this paper assume a Kroupa IMF (Kroupa 2001).

2.2.1. SFRs using FUV and 24 μ m Observations

To estimate SFRSD maps of the seven galaxies in Sample 1 (Table 2) using FUV+24 μ m emission, we used SPITZER 24 μ m IR data (Dale et al. 2009) and GALEX FUV data (11HUGS survey; Kennicutt et al. 2008). We first convolved both the 24 μ m and the FUV maps of all galaxies to the same resolutions as our magnetic field maps. The FUV data were corrected for extinction due to dust in the Milky Way (see Section 2.2.4). The FUV images were in units of counts/sec/pixel and were converted to flux-density units of MJy Sr⁻¹. We also converted the 24 μ m images to units of MJy Sr⁻¹ and used the following calibration from Leroy et al. (2012) to derive SFRSD maps for the sample galaxies:

$$\Sigma_{\text{SFR}}[\text{M}_{\odot}\text{yr}^{-1}\text{kpc}^{-2}] = 0.081 I_{\text{FUV}}[\text{MJy sr}^{-1}] + 0.032 I_{24\mu\text{m}}[\text{MJy sr}^{-1}] \quad (2)$$

The uncertainties of the coefficients are ~ 10 -30%. Note that the uncertainty in SFR estimates arises from issues such as the error in sampling the stellar IMF of different star-forming regions, determining the contribution of different emission which are not associated with recent star formation, etc. (e.g Kennicutt & Evans 2012b; Leroy et al. 2012).

2.2.2. SFRs using H α and 24 μ m Observations

To estimate SFRSD maps using H α +24 μ m as a tracer, we used 24 μ m emission along with H α emission from 11HUGS (Kennicutt et al. 2008), for all but NGC 5194, for which we used data from the SINGS survey (Kennicutt et al. 2003). All the maps were convolved and regridded to the resolution and pixel size of the magnetic field maps. For the H α maps from 11HUGS and SINGS, the flux density units were converted to erg/s/cm². We used the following calibration from Leroy et al. (2012) to estimate SFRSDs of the galaxies in Sample 1.

$$\Sigma_{\text{SFR}}[\text{M}_{\odot}\text{yr}^{-1}\text{kpc}^{-2}] = 634.0 I_{\text{H}\alpha}[\text{erg s}^{-1} \text{sr}^{-1}] + 0.0025 I_{24\mu\text{m}}[\text{MJy sr}^{-1}] \quad (3)$$

2.2.3. SFRs using 1.4 GHz Observations

Our 1.4 GHz non-thermal maps of the galaxies (Sample 1) (Roy & Manna 2021) and an SFR calibration from Murphy et al. (2011) were used to derive SFRSD maps (Equation 4). The calibration is based on the observed radio-FIR correlation in a sample of nearby star-forming galaxies (Bell 2003) and has a scatter of 0.26 dex. We used this galaxy-integrated calibration (Equation 4) to derive the formula for spatially-resolved radio- Σ_{SFR} calibration.

$$\frac{\text{SFR}_{1.4\text{GHz}}}{\text{M}_{\odot}\text{yr}^{-1}} = 6.35 \times 10^{-29} \frac{L_{1.4\text{GHz}}}{\text{erg Hz}^{-1}\text{s}^{-1}} \quad (4)$$

The spatially-resolved calibration is consistent with the calibration of Heesen et al. (2014). We used the above relation to estimate the SFRSD maps of the sample galaxies from the measured 1.4 GHz surface brightness.

2.2.4. Galactic Extinction Correction for FUV Emission

We corrected for the extinction of FUV emission due to dust in the Milky Way using the E(B-V) values along the line of sight to the sample galaxies from Bianchi et al. (2017). The extinction coefficients (A_{FUV}) of the GALEX FUV bands were measured using Table 1 from Bianchi et al. (2017) and intrinsic fluxes ($F_{\text{intrinsic}}$) were estimated from the following formula:

$$A_{\text{FUV}} = -2.5 \times \log\left[\frac{F_{\text{observed}}}{F_{\text{intrinsic}}}\right] \quad (5)$$

The extinction percentage of the FUV emission is listed in Table 3.

2.3. Gas Densities

Atomic hydrogen (HI) and molecular hydrogen (H₂) predominantly contribute to the total gas mass of galaxies. H₂ is best traced using rotational transitions in CO (e.g. Bolatto et al. 2013). Spatially-resolved observations of CO transitions exist for only three of our seven galaxies in Sample 1 (Table 2). We have used CO J=2-1 line data of NGC 3627 and NGC 5194 from the HERA CO-Line Extragalactic Survey (HERACLES; Leroy et al. 2009) and CO J=1-0 data of NGC 4826 from the BIMA Survey of Nearby Galaxies (BIMA SONG; Regan et al. 2001). The HERACLES and BIMA survey have a spatial resolution of 13'' and 6'', respectively. The velocity resolution of the HERACLES and BIMA spectral cubes are ~ 5 and 6 km/s, respectively. We restrict our study of the connection between gas densities and magnetic fields to only these three galaxies for which spatially-resolved CO data are available.

Table 3. FUV extinction values of the Sample 1 galaxies due to the Milky Way foreground dust. The extinctions were computed using E(B-V) values along the line of sight to the sample galaxies from Bianchi et al. (2017).

Name	Percentage extinction
NGC 2683	22
NGC 3627	23
NGC 4096	21
NGC 4449	15
NGC 4490	15
NGC 4826	13
NGC 5194	27

The HI Nearby Galaxy Survey (THINGS; Walter et al. 2008) used VLA observations to obtain very high spectral (≤ 5.2 km/s) and spatial ($\sim 6''$) resolution maps of nearby galaxies at 21cm. We used the publicly available 21cm moment maps from this THINGS survey to estimate the distribution of HI in the three galaxies for which CO data are available. All CO and HI 21 cm maps were convolved and regridded to a common resolution and pixel size of the non-thermal radio maps. Gas densities were estimated (for NGC 3627, NGC 4826 and NGC 5194) following Basu & Roy (2013) assuming CO to H₂ conversion factor of 2×10^{20} (K km s⁻¹)⁻¹ (e.g. Bolatto et al. 2013). A line ratio of 0.8 was assumed to convert CO_{J=2-1} to CO_{J=1-0} (e.g. Leroy et al. 2009). We accounted for the contribution of helium to the gas density using $\rho_{\text{gas}} = 1.36 \times (\rho_{\text{HI}} + \rho_{\text{H}_2})$. Line of sight depths were assumed to be 300 and 400 pc for molecular and atomic gas, respectively (Basu & Roy 2013).

3. RESULTS

3.1. Magnetic Fields in the Galaxies

We have estimated spatially resolved revised equipartition magnetic field maps for seven galaxies in Sample 1, using the procedures of Section 2.1; these maps are shown in Figures 1 & 2. Flux density contours of 1.4 GHz observations are overlaid on magnetic field maps. The resolution of these maps corresponds to spatial scales of ~ 0.4 – 0.8 kpc (see Table 1). The bottom right panel of Figure 2 shows the radial variation of the magnetic field with galactocentric radius of all the seven galaxies where both the axes are normalized by their maximum values. Here, we have averaged the magnetic field strengths over an annular elliptical region of width equal to the beam size of the corresponding map. Position and inclination angle (Table 1) of each galaxy were used while selecting the elliptical regions. We find magnetic fields to be stronger at the central region and at the star formation sites (arm regions) with field strengths up to 50 μ G. Field strengths fall by $\sim 50\%$ at the edges of the magnetic field maps. The Milky Way also shows such a trend in the variation of magnetic field strengths (Beck et al. 1996). We note that our analysis was limited to distances where the signal-to-noise ratio in spectral index maps is > 5 ; the magnetic field strengths at these distances are thus likely to be reliable.

We note that, compared to the magnetic field strengths obtained using the classical equipartition expression, these values are higher by ~ 1.3 – 1.5 for a non-thermal spectral index of -0.6 , and they match for a spectral index of -0.75 (Beck & Krause 2005).

Figure 7 shows the uncertainties in the magnetic field values for Sample 1 derived using the Monte Carlo method described in Section 2.1.1. Statistical uncertainties on mean magnetic fields for these seven galaxies are provided in Table 4.

3.2. Star Formation Rates in the Galaxies

We have estimated the global, galaxy-averaged SFRs of Sample 1 galaxies using 1.4 GHz, FUV+24 μ m, and H α +24 μ m emission using calibrations discussed in Section 2.2. Globally integrated star formation rates of the sample galaxies are given in Table 5. No systematic offset was found in the SFR values estimated using these tracers. The differences in the SFR values for our galaxies are much less than the calibration uncertainty except for NGC 4490. For NGC 4490, SFR calculated from 1.4 GHz emission is higher than the same from FUV+24 μ m emission by a factor of 2.2.

As discussed in Section 2.2, we have estimated SFRSD maps of the seven galaxies (Sample 1) using FUV+24 μ m, H α +24 μ m and 1.4GHz emission. We show SFRSD maps of the seven galaxies in the Appendix (Figures 8-9), where SFRSDs estimated using 1.4 GHz and FUV+24 μ m emission are shown in contours and colors, respectively. In the

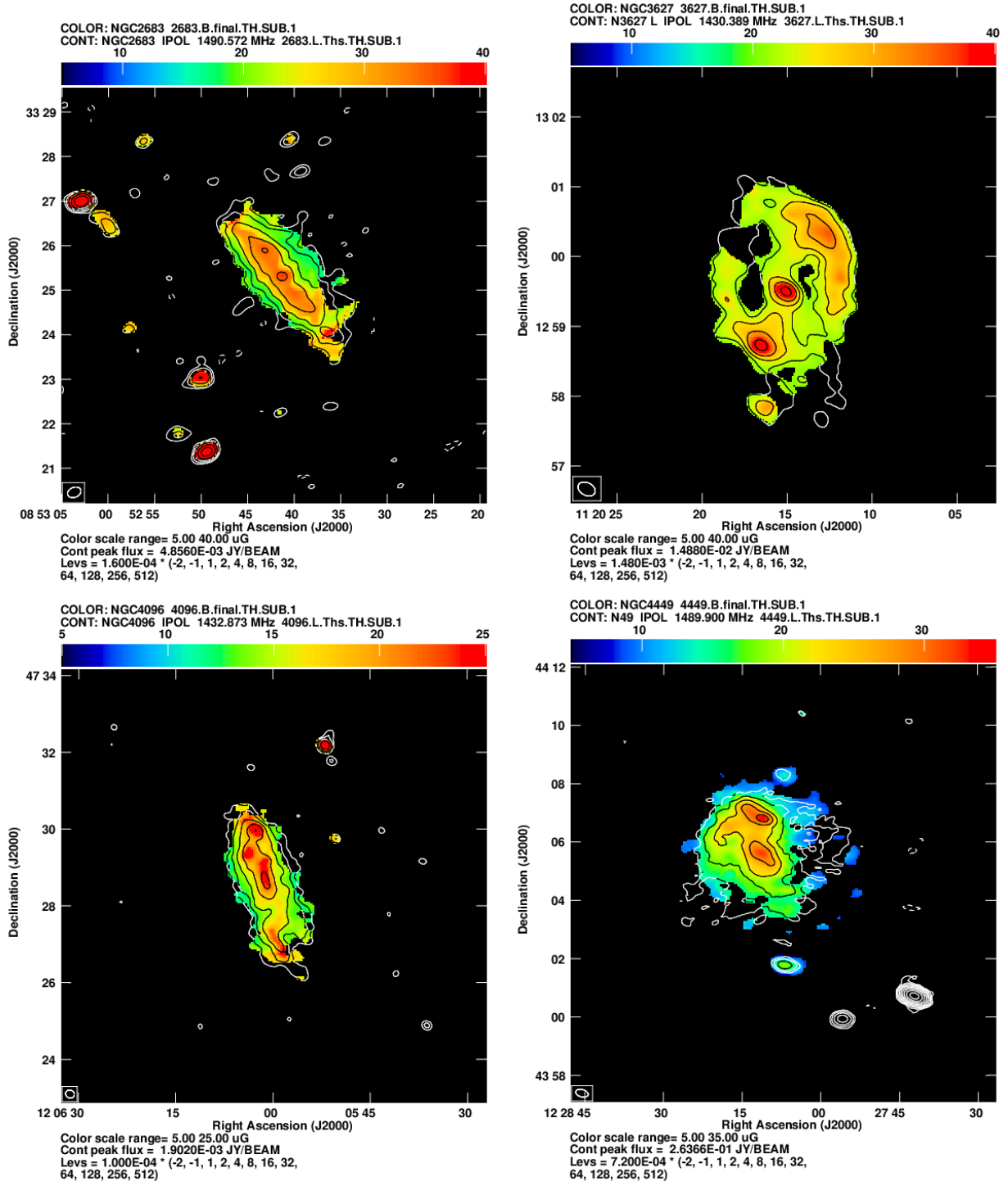


Figure 1. The equipartition magnetic field maps of NGC 2683, NGC 3627, NGC 4449 and NGC 4096 (clockwise from top left) (Sample 1). Non-thermal radio contours at 1.4 GHz are overlaid on magnetic field maps. The magnetic field strengths are shown in color with non-thermal emission at 1.4 GHz shown as overlaid contours. Contour levels are presented below each panel in the figure. The circle in the bottom-left corner of the panels indicates the angular resolution of the maps. The uncertainties on mean magnetic fields are $0.06\mu\text{G}$, $0.17\mu\text{G}$, $0.04\mu\text{G}$ and $0.18\mu\text{G}$ for the above galaxies, respectively.

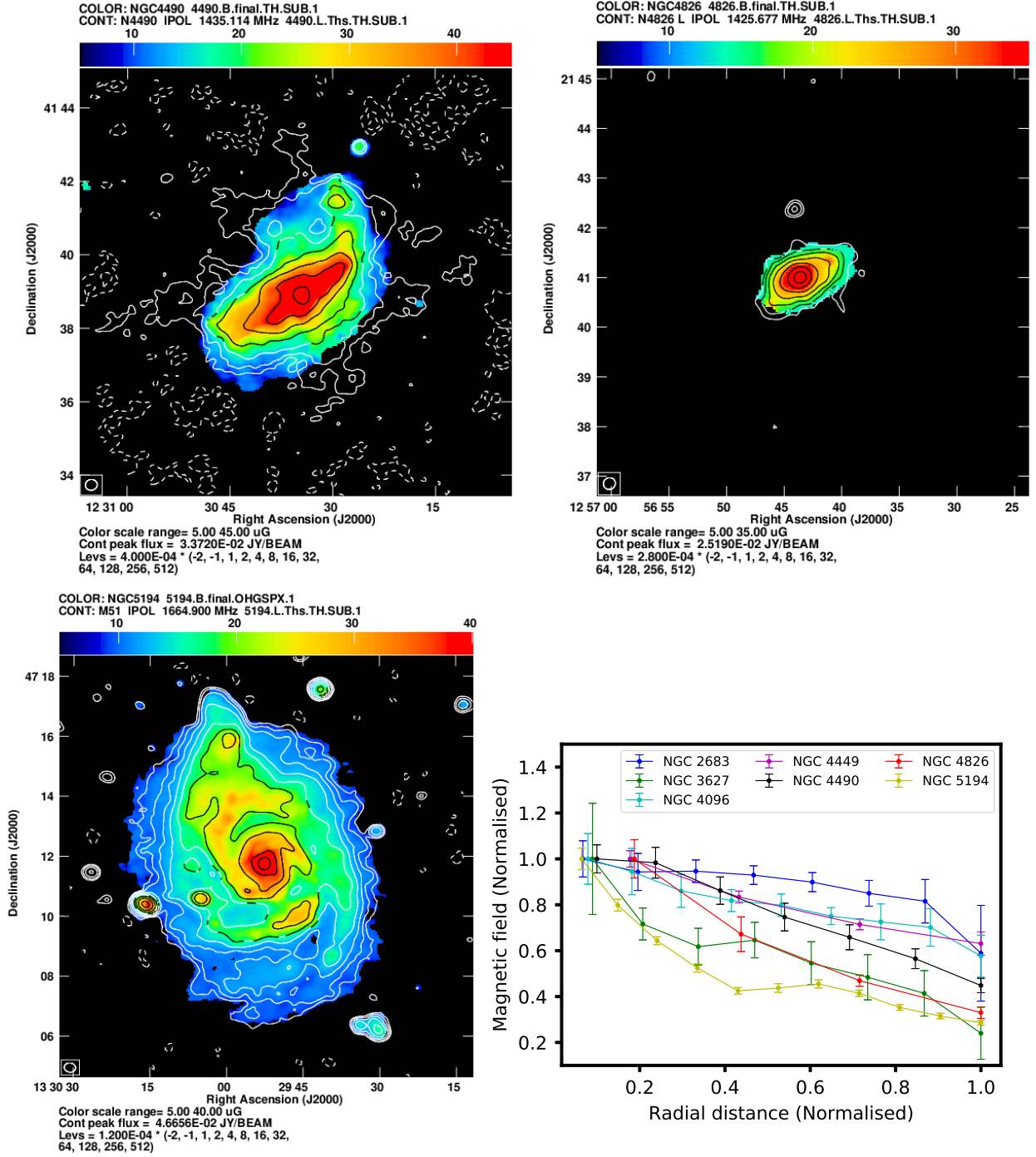


Figure 2. The equipartition magnetic field maps of NGC 4490 (top left), NGC 4826 (top right) and NGC 5194 (bottom left). The magnetic field strengths are shown in color with non-thermal emission at 1.4 GHz shown as overlaid contours. Contour levels are presented below each panel in the figure. The circle in the bottom-left corner of the panels indicates the angular resolution of the maps. The uncertainties on mean magnetic fields are $0.06\mu\text{G}$, $0.11\mu\text{G}$ and $0.02\mu\text{G}$, respectively. The bottom right panel presents the radial variation of magnetic field strengths with galactocentric distance for all seven galaxies in Sample 1.

Table 4. Statistical uncertainties on mean magnetic fields for galaxies in Sample 1.

Name	Statistical uncertainty on mean magnetic fields (μG)
NGC 2683	0.06
NGC 3627	0.17
NGC 4096	0.04
NGC 4449	0.18
NGC 4490	0.06
NGC 4826	0.11
NGC 5194	0.02

Table 5. Galaxy-averaged star formation rates of the galaxies in Sample 1, using 1.4 GHz, FUV+24 μm , and H α +24 μm data. The uncertainties on the SFR values are $\approx 30\%$.

Name	SFR from 1.4 GHz ($\text{M}_{\odot}\text{yr}^{-1}$)	SFR from FUV+24 μm ($\text{M}_{\odot}\text{yr}^{-1}$)	SFR from H α +24 μm ($\text{M}_{\odot}\text{yr}^{-1}$)
NGC 2683	0.28	0.25	0.33
NGC 3627	1.56	2.00	1.84
NGC 4096	0.42	0.35	0.38
NGC 4449	0.37	0.38	0.32
NGC 4490	4.63	2.13	2.30
NGC 4826	0.63	0.73	0.78
NGC 5194	4.16	3.88	3.65

Appendix (Figures 10-11), we also present the SFRSD maps estimated using H α +24 μm and 1.4 GHz emission in colors and contours, respectively. The SFRSD maps of each galaxy in Figures 8–11 are shown in the same color scale and contours. To determine the radial variation of SFRSDs, we have averaged the SFRSD maps of our sample galaxies over tilted rings centred on the optical centre of each galaxy using their inclinations and position angles. The width of the tilted rings was taken to be equal to the beam size of the corresponding image. Figure 3 shows the radial variation of the average SFRSD, derived using FUV+24 μm and H α +24 μm emission, with galactocentric distance where both the axes are normalized to their maximum values. We also derived the radial variation of SFRSDs for the galaxies using 1.4 GHz emission and it is consistent within 1σ statistical uncertainties, with those derived using FUV+24 μm and H α +24 μm data. Azimuthally averaged SFRSDs of all the seven galaxies decrease gradually towards the outer region and drop by a factor of 6 to 8 at the edge.

3.3. Details of the Individual Galaxies of Sample 1

(i) NGC 2683: In this galaxy, Krause et al. (2020) found very weak linear polarisation using C-band and L-band VLA observations. Based on the optical image, we could separate the central region from the disk. The average magnetic field in the central region is found to be $\approx 31 \mu\text{G}$ and the outer region of the disk has an average value of $\approx 19 \mu\text{G}$ (see Figure 1 and Table 6).

Wiegert et al. (2015) used WISE 22 μm data to estimate a galaxy-averaged SFR of $\approx 0.09 \text{ M}_{\odot}\text{yr}^{-1}$ for NGC 2683. From our analysis, integrated SFR was measured to be $\sim 0.24 \text{ M}_{\odot}\text{yr}^{-1}$ and $\sim 0.28 \text{ M}_{\odot}\text{yr}^{-1}$ using FUV+24 μm and 1.4 GHz radio emission, respectively. However, we note that Wiegert et al. (2015) used a distance of 6.27 Mpc for this galaxy, but we have used a distance of 7.7 Mpc. The SFR is estimated to be $0.16 \text{ M}_{\odot}\text{yr}^{-1}$ using FUV+24 μm emission, assuming the same distance as used by Wiegert et al. (2015). Taking the calibration uncertainties and the assumed distance into account, our estimated SFR is hence consistent with that of Wiegert et al. (2015). We note that the contours on the background sources (Figure 8) are not real SFRSDs, as these are likely to be background AGNs.

(ii) NGC 3627: NGC 3627 was observed at 8.46 GHz and 4.85 GHz using the VLA in its D-configuration (Soida et al. 2001). These authors estimated the magnetic field strengths using the classical equipartition formula (Longair 2011) and found an average equipartition magnetic field strength of $11 \pm 2 \mu\text{G}$, assuming a constant non-thermal spectral

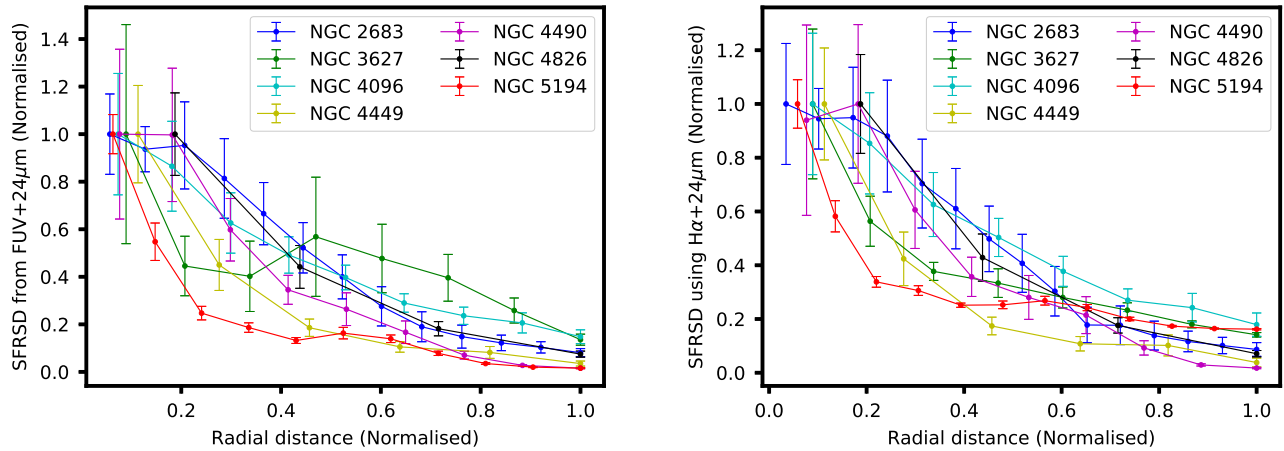


Figure 3. The variation of SFRSDs (normalized), estimated using FUV+24 μ m (left panel) and H α +24 μ m (right panel) emission as a function of galactocentric distance (normalized) for all seven galaxies in Sample 1.

index of 0.9 and a disk thickness of 2 kpc. [Soida et al. \(2001\)](#) also studied the polarized emission at these frequencies to find a regular magnetic field of $4 \pm 1 \mu\text{G}$. They suggested two distinct magnetic field components of NGC 3627: one for the spiral arms and another for the inter-arm regions. We have separately studied equipartition magnetic fields in the arm and interarm regions of the galaxy. We find that the central region and the edges of the extended bar have magnetic field strengths of $\approx 34 \mu\text{G}$ (see Figure 1). The arm region has a field strength of $\approx 28 \mu\text{G}$ (see Table 6). However, the magnetic field strength in the interarm regions has values $\approx 21 \mu\text{G}$. We note that our estimates of the equipartition magnetic field strengths in the galaxy are higher than those found by [Soida et al. \(2001\)](#); this difference likely arises from the fact that [Soida et al. \(2001\)](#) estimated the magnetic field strengths using the classical equipartition formula, which is known to significantly underestimate the magnetic field in the star-forming regions.

We measured a galaxy-averaged SFR of $\approx 2.0 \text{ M}_{\odot} \text{ yr}^{-1}$ and $\approx 1.56 \text{ M}_{\odot} \text{ yr}^{-1}$ from FUV+24 μ m and 1.4 GHz emission, respectively. Our measurements of spatially resolved SFRs in different regions are consistent, within calibration uncertainties, with the SFR estimates of [Watanabe et al. \(2011\)](#).

(iii) **NGC 4096:** Our estimate of the equipartition magnetic field in NGC 4096 varies from $\approx 21 \mu\text{G}$ at the centre to $\approx 12 \mu\text{G}$ at the edge (table 6). The magnetic field strength in both the central region and northern periphery is quite similar, with typical field strengths of $\approx 20 \mu\text{G}$; this is presumably due to its high inclination. The outer part of the galaxy has an average field strength of $\approx 14 \mu\text{G}$. NGC 4096 was observed ([Irwin et al. 2012](#); [Wiegert et al. 2015](#)) with its B-field and further studied by [Krause et al. \(2020\)](#) who found very little polarized emission from the galaxy.

[Wiegert et al. \(2015\)](#) used the 22 μm –SFR calibration to measure a galaxy-averaged SFR of $0.27 \pm 0.02 \text{ M}_{\odot} \text{ yr}^{-1}$. Our measurement of the galaxy-averaged SFR is $\approx 0.35 \text{ M}_{\odot} \text{ yr}^{-1}$ and $\approx 0.43 \text{ M}_{\odot} \text{ yr}^{-1}$ using FUV+24 μ m and 1.4 GHz emission, respectively. Considering the calibration uncertainties, our estimates are consistent with that of [Wiegert et al. \(2015\)](#).

(iv) **NGC 4449:** This is an optically bright irregular starburst galaxy. [Chyży et al. \(2000\)](#) used VLA 4.86 and 8.46 GHz observations to find a galaxy-averaged equipartition magnetic field of $\approx 14 \mu\text{G}$. These authors also used polarization emission to estimate a regular field of $\approx 8 \mu\text{G}$. The equipartition magnetic field map of NGC 4449 from our study is shown in Figure 1. As noted in Section 2.1, about 70 % of the total projected area of this galaxy has spectral index values of less than 0.55. We have replaced the pixel values with $\alpha_{\text{nt}} < 0.55$ with $\alpha_{\text{nt}} = 0.55$ while computing the magnetic field for NGC 4449 (see Section 2.1). The average magnetic field strength is $\approx 17 \mu\text{G}$ in this galaxy, which is comparable to the findings of [Chyży et al. \(2000\)](#).

Our measurements of the galaxy-averaged SFR are $\approx 0.38 \text{ M}_{\odot} \text{ yr}^{-1}$ and $\approx 0.37 \text{ M}_{\odot} \text{ yr}^{-1}$ using FUV+24 μ m and 1.4 GHz emission, respectively, which are consistent with the SFR of $0.47 \text{ M}_{\odot} \text{ yr}^{-1}$ estimated by [Chyży et al. \(2011\)](#).

(v) **NGC 4490:** [Nikiel-Wroczyński et al. \(2016\)](#) observed NGC 4490 at 0.61 GHz using the GMRT, and at 4.86 & 8.44 GHz using VLA + Effelsberg. The authors used these observations to find a mean equipartition magnetic field

Table 6. Magnetic field strengths in different regions of the galaxies in Sample 1. For the irregular galaxy NGC 4449, we could only measure the galaxy-integrated magnetic field. We have separated the two nearly face-on galaxies (NGC 3627 and NGC 5194) into arm and inter-arm regions. For the rest of the galaxies, we could not separate the arm and inter-arm region due to their higher inclinations.

Galaxy name	Galaxy-average B_{eq} (μG)	B_{eq} in central region (μG)	B_{eq} in disk region (μG)	B_{eq} in arm region (μG)	B_{eq} in inter-arm region (μG)
NGC 2683	24 \pm 6	31 \pm 3	19 \pm 5	–	–
NGC 3627	25 \pm 4	34 \pm 8	–	28 \pm 5	21 \pm 4
NGC 4096	16 \pm 4	21 \pm 5	14 \pm 3	–	–
NGC 4449	17 \pm 6	–	–	–	–
NGC 4490	23 \pm 10	40 \pm 6	17 \pm 7	–	–
NGC 4826	23 \pm 9	38 \pm 8	20 \pm 5	–	–
NGC 5194	16 \pm 6	34 \pm 6	–	25 \pm 5	18 \pm 4

of $21.9\pm 2.9 \mu\text{G}$, with typical field strengths in the range of $18 \mu\text{G}$ to $40 \mu\text{G}$. We have found a typical equipartition magnetic field strength of $\approx 40 \mu\text{G}$ in the central region, which decreases to $\approx 17 \mu\text{G}$ in the outer region (see Figure 2); these values are consistent with the estimates of [Nikiel-Wroczyński et al. \(2016\)](#). We find a relatively lower magnetic field strength of $\approx 15 \mu\text{G}$ in both the interacting region and the companion galaxy NGC 4485. Therefore, a gradual decrease in the average magnetic field strength occurs from the center to the outer region.

[Clemens et al. \(1999\)](#) used radio observations to find a galaxy-averaged SFR of $4.7 M_{\odot}\text{yr}^{-1}$. We found a similar SFR ($\approx 4.63 M_{\odot}\text{yr}^{-1}$) using 1.4 GHz radio emission but a factor of ~ 2 lower SFR ($2.13 M_{\odot}\text{yr}^{-1}$) using the FUV+ $24\mu\text{m}$ emission (Table 5). Extinction corrections for NGC 4490 are believed to be higher than those typically assumed and this may lead to an underestimation of the SFR while using the FUV+ $24\mu\text{m}$ diagnostics ([Clemens et al. 1999](#)).

(vi) NGC 4826: No spatially resolved maps of magnetic fields and SFRSDs are available in the literature. We measure the central and outer regions of the galaxy to have an average equipartition magnetic field strength of $\approx 38 \mu\text{G}$ and $\approx 20 \mu\text{G}$, respectively (see Figure 2 and Table 6). We find galaxy-averaged SFR of $\approx 0.73 M_{\odot}\text{yr}^{-1}$ and $\approx 0.63 M_{\odot}\text{yr}^{-1}$ using FUV+ $24\mu\text{m}$ and 1.4 GHz data, respectively.

(vii) NGC 5194: [Fletcher et al. \(2011\)](#) used VLA C-band observations of the galaxy and assumed a constant thermal and non-thermal spectral index of 0.1 and 1.1 to find an average equipartition magnetic field strength of $20 \mu\text{G}$ using the revised formula by [Beck & Krause \(2005\)](#). They found a magnetic field of $20\text{--}25 \mu\text{G}$ in the spiral arms, higher than the $15\text{--}20 \mu\text{G}$ typical in the interarm regions. Using VLA observations at S-band ($2\text{--}4 \text{GHz}$) frequencies, [Kierdorf et al. \(2020\)](#) found the field strength of turbulent and regular components of the magnetic field in the arm regions of $18\text{--}24 \mu\text{G}$ and $8\text{--}16 \mu\text{G}$, respectively. We find an equipartition magnetic field strength of $\approx 25 \mu\text{G}$ in the arm region and $\approx 18 \mu\text{G}$ in the interarm region (see Table 6). The peripheral region has a magnetic field of $\approx 12 \mu\text{G}$, while the overlapping region between NGC 5194 and NGC 5195 has an average B_{eq} of $\approx 16 \mu\text{G}$. Considering our use of Equation 1 ([Beck & Krause 2005](#)), measurements are roughly consistent with the earlier study of [Fletcher et al. \(2011\)](#) and [Kierdorf et al. \(2020\)](#).

Spatially resolved SFRs were measured in several star-forming regions of NGC 5194 using $\text{H}\alpha$ + $24\mu\text{m}$ and $\text{H}\alpha$ + $\text{Pa}\alpha$ emission ([Kennicutt et al. 2007](#)). SFRSDs in different regions were found to be in the range of 0.10 to $0.46 M_{\odot}\text{yr}^{-1}\text{kpc}^{-2}$. Our estimates using the two tracers are consistent with the estimates of [Kennicutt et al. \(2007\)](#) (See Figures 9 & 11). Furthermore, we find that the galaxy-integrated SFR derived using FUV+ $24\mu\text{m}$ ($\approx 3.88 M_{\odot}\text{yr}^{-1}$) and 1.4 GHz data ($\approx 4.16 M_{\odot}\text{yr}^{-1}$) are consistent with each other, within 1-sigma statistical uncertainty.

3.4. Is the Minimum Energy Condition Valid for the Sample Galaxies?

We have estimated magnetic fields for the galaxies in Sample 1 assuming the “minimum energy condition” or “equipartition condition”, i.e. by assuming that the energy density in the magnetic field is approximately equal to the energy density in cosmic ray particles. Therefore, it is important to verify the validity of this assumption in our sample galaxies. The tightness of the spatially-resolved radio–FIR correlation can be used to estimate the deviation of the energy densities from the minimum energy condition ([Hummel 1986](#); [Basu & Roy 2013](#)). According to the simplified model of [Hummel \(1986\)](#), when the minimum energy condition is satisfied, the distribution of $I_{\text{nt}}/I_{\text{FIR}}$ will be similar to the distribution of $B^{1+\alpha_{\text{nt}}}$. The model assumes the following to be constant across galaxies: (a) the ratio of the number densities of relativistic electrons and dust-heating stars, (b) the volume ratio of radio and FIR emitting

regions, and (c) the ratio of efficiency factors for both the radio and FIR emission. In this model, the cumulative distribution function (CDF) of the quantity $I_{\text{nt}}/I_{\text{FIR}}$ and $B_{\text{eq}}^{1+\alpha_{\text{nt}}}$ is expected to follow each other if B_{eq} is close to B .

To verify the validity of the minimum energy condition in our sample galaxies, we have followed the procedure as in Hummel (1986) and Basu & Roy (2013). The CDF of $I_{\text{nt}}/I_{\text{FIR}}$ and $B_{\text{eq}}^{1+\alpha_{\text{nt}}}$ were estimated using our radio maps of the sample galaxies at both 0.33 and 1.4 GHz. We used an ensemble of spatially-resolved values of α_{nt} , I_{nt} (both at 0.33 and 1.4 GHz), I_{FIR} (70 μm) and magnetic fields (B_{eq}), which are averaged over the beam size from all the galaxies in Sample 1 (Table 2) to generate these distributions. The CDFs of all quantities were normalized by their median values. The top panels in Figure 4 show the median-normalized CDFs of $I_{\text{nt}}/I_{\text{FIR}}$ and $B_{\text{eq}}^{1+\alpha_{\text{nt}}}$ at both 0.33 and 1.4 GHz.

We find that the CDFs of $I_{\text{nt}}/I_{\text{FIR}}$ and $B_{\text{eq}}^{1+\alpha_{\text{nt}}}$ at both 0.33 and 1.4 GHz broadly follow each other but with slight deviations at high and low ends (see top panels in Figure 4). This implies that the minimum energy condition is broadly valid and is consistent with earlier findings. For example, Hummel (1986) found the distribution of the two quantities is similar in a sample of Sbc galaxies while Basu & Roy (2013) reached similar conclusions in a study of 5 nearby large spiral galaxies, but with slight deviations observed in the CDFs of $I_{\text{nt}}/I_{\text{FIR}}$ and $B_{\text{eq}}^{1+\alpha_{\text{nt}}}$ in the interarm regions of the galaxies.

The observed deviation in the CDFs of $I_{\text{nt}}/I_{\text{FIR}}$ and $B_{\text{eq}}^{1+\alpha_{\text{nt}}}$ for our sample galaxies imply a corresponding deviation from the minimum-energy condition. In order to quantify this deviation, we performed a Monte Carlo simulation originally proposed by Hummel (1986). In this simulation, random numbers (X) were drawn from a Gaussian distribution with standard deviation σ . Thereafter, we multiplied 10^X with the observed equipartition magnetic fields to introduce deviations from the minimum-energy condition. We thus constructed the CDF of $B_{\text{eq}}^{1+\alpha_{\text{nt}}}$ using the deviated magnetic field values. The CDF of $B_{\text{eq}}^{1+\alpha_{\text{nt}}}$ were then compared to the observed CDF of $I_{\text{nt}}/I_{\text{FIR}}$ via a Kolmogorov-Smirnov (KS) test. This procedure was repeated for a range of σ from 0 to 0.2. We find that the p-values for the KS test comparing the distributions are maximized when $\sigma = 0.1$. Indeed, $B_{\text{eq}}^{1+\alpha_{\text{nt}}}$ derived after deviating the magnetic field using $\sigma = 0.1$ and $I_{\text{nt}}/I_{\text{FIR}}$ are consistent with being derived from the same distribution, with a KS test p-value of 0.41 and 0.55, when using I_{nt} at 0.33 and 1.4 GHz, respectively. The bottom panels in Figure 4 show the CDFs of the two quantities for $\sigma = 0.1$ at 0.33 and 1.4 GHz; it is clear that the CDFs follow each other. This implies the actual magnetic field values may deviate from the equipartition values by $\sim 25\%$ in our galaxies in Sample 1. We note that any violation of the assumptions made by Hummel (1986) may also lead to the observed deviation in the CDFs.

3.5. Correlation Between Magnetic Fields and SFRSDs

We have studied the correlation between the spatially-resolved equipartition magnetic field and SFRSDs for the galaxies in Sample 1 (Table 2) at scales of $\approx 360\text{--}760$ pc (Table 1). For the seven sample galaxies, we used the SFRSD maps estimated using the FUV+24 μm emission. The correlations between magnetic fields and SFRSDs for the seven galaxies are shown in Figure 5. Each point represents the logarithms of equipartition magnetic fields and SFRSD values that are averaged over the beam size of the corresponding maps. da Silva et al. (2014) found that SFR calibrations could be biased and strongly affected by stochasticity at small spatial scales where the star formation rate is low ($\leq 10^{-2.5} \text{ M}_{\odot}\text{yr}^{-1}$); we have therefore excluded regions of low star formation rates from the correlation study.

We find that the equipartition magnetic field and the SFRSD are correlated in all seven sample galaxies. We use *orthogonal distance regression* in Scipy (Virtanen et al. 2020) to fit a power law of the form $B = B_0 (\Sigma_{\text{SFR}})^{\eta}$ to the magnetic field – SFRSD data points; the spatially-resolved uncertainty maps of equipartition magnetic fields and rms noise on the SFRSD maps were used to estimate the uncertainties on each data point during the fitting procedure. The best-fit parameters of the power-law are given in Table 7. We have also estimated the scatter (rms of the data points along the y-axis) of the correlations which are presented in Table 7 and are shown in dashed lines in the corresponding plots (Figure 5). We find that six of the seven galaxies have slopes (η) in the range of $\approx 0.27\text{--}0.40$ but that the slope is relatively lower for NGC 4449 with $\eta \approx 0.18$. Averaging over the slope of all galaxies in Sample 1, we find a mean slope of 0.32 ± 0.06 .

3.6. Correlation Between Magnetic Fields and Gas Densities

We have studied the correlation between spatially-resolved equipartition magnetic fields and gas densities for three of the galaxies in Sample 1, NGC 3627, NGC 4826, and NGC 5194, for which spatially resolved CO observations were available (see Section 2.3). Similar to the study of correlations between B_{eq} and SFRSDs, we have studied the correlations between B_{eq} and gas density values, both averaged over the beam size of the corresponding maps. The

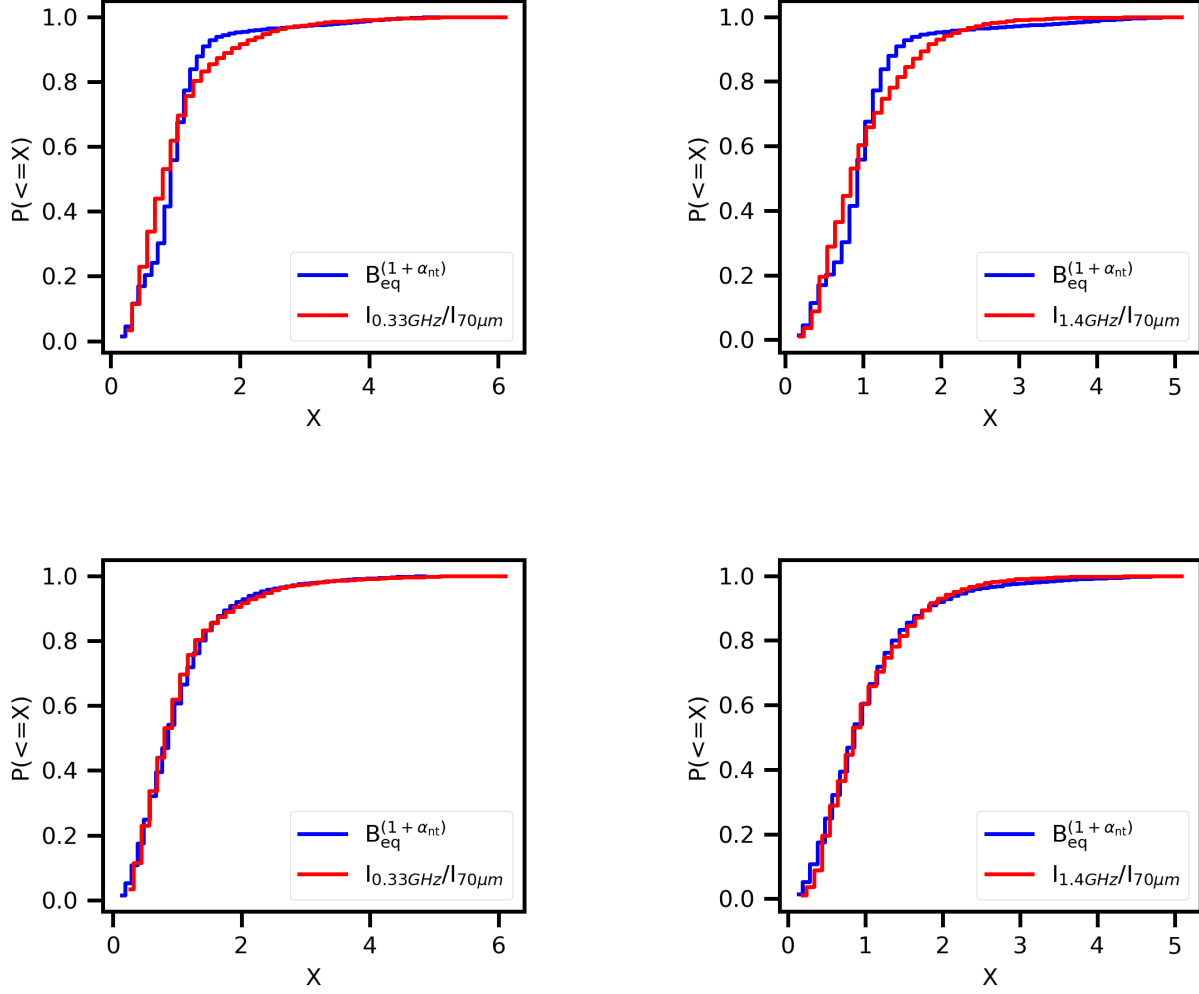


Figure 4. The top panels show the cumulative distribution function (CDF) of $I_{\text{nt,radio}}/I_{70\mu\text{m}}$ (in red) and $B_{\text{eq}}^{1+\alpha_{\text{nt}}}$ (in blue), where I_{nt} is the non-thermal emission at 0.33 GHz (top left) and 1.4 GHz (top right) (Sample 1). The variables are normalized by their median values. The bottom panels show the same but now with the magnetic field perturbed from its measured value using $\sigma=0.1$ (see Section 3.4); the CDFs of the $I_{\text{nt,radio}}/I_{70\mu\text{m}}$ and $B_{\text{eq}}^{1+\alpha_{\text{nt}}}$ are now consistent with being derived from the same distribution.

Table 7. Best-fit parameters and the scatter of the correlation between magnetic fields and SFRSDs for the seven galaxies in Sample 1. The data were fitted with a power law of the form $B=B_0(\Sigma_{\text{SFR}})^\eta$.

Name	Slope (η)	Intercept (B_0) ($\log(\mu\text{G})$)	Intercept (B_0) (μG)	Scatter
NGC 2683	0.34 ± 0.04	2.10 ± 0.07	125 ± 1.2	0.05
NGC 3627	0.31 ± 0.03	1.71 ± 0.03	51 ± 1.1	0.04
NGC 4096	0.33 ± 0.04	1.80 ± 0.08	63 ± 1.2	0.05
NGC 4449	0.18 ± 0.03	1.64 ± 0.04	43 ± 1.1	0.03
NGC 4490	0.27 ± 0.02	1.90 ± 0.03	79 ± 1.1	0.06
NGC 4826	0.38 ± 0.02	1.80 ± 0.02	63 ± 1.0	0.05
NGC 5194	0.40 ± 0.01	2.00 ± 0.02	100 ± 1.0	0.07

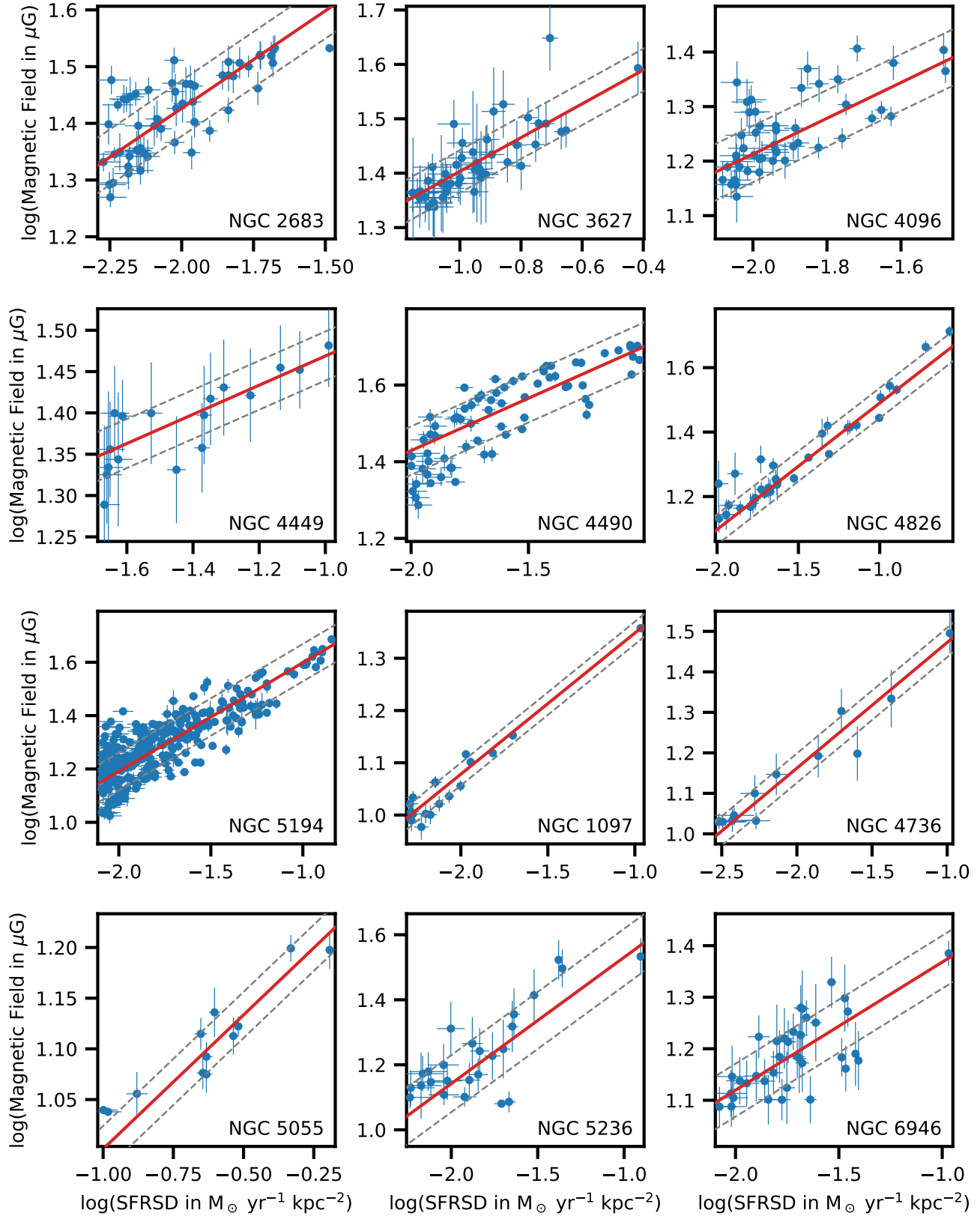


Figure 5. The correlation between magnetic fields and SFRSD for the combined sample of 12 galaxies (Sample 2, Table 2). For the seven galaxies in Sample 1, the SFRSD estimates shown in the plots were derived using FUV + $24\mu\text{m}$ (Section 3.5). The SFRSD estimates for the five galaxies from Basu et al. (2012a) (Sample 2) were derived using H α + $24\mu\text{m}$ (Section 4). The red line shows a linear fit to the data points. The black dashed lines show the $\pm 1\sigma$ vertical scatter.

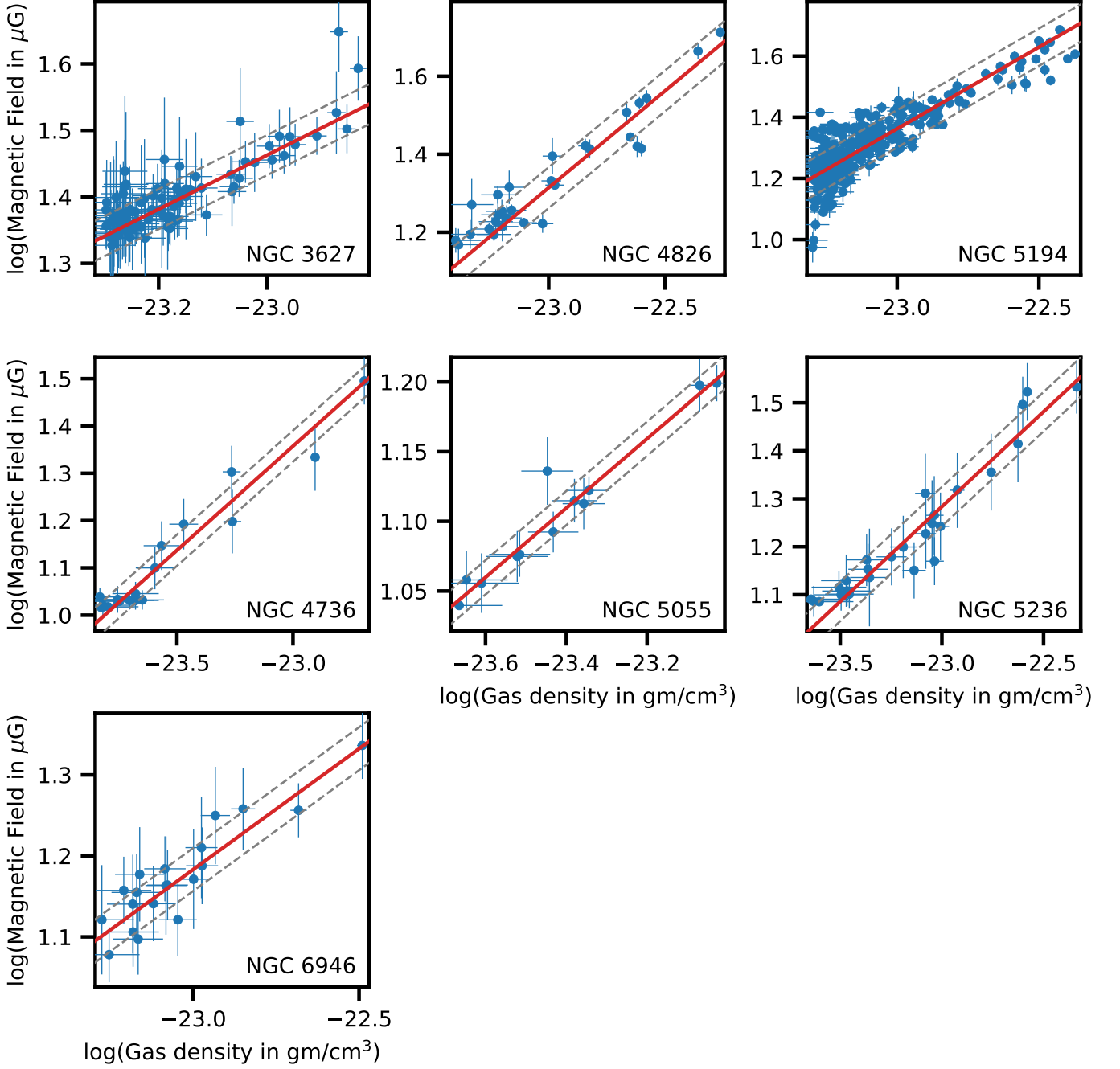


Figure 6. The correlations between magnetic fields (μG) and gas densities (gm/cm^{-3}) for seven galaxies of Sample 3 (Table 2). The red line shows a linear fit to the data points. The black dashed lines show the $\pm 1\sigma$ vertical scatter.

correlations between magnetic fields and gas densities of NGC 3627, NGC 4826, and NGC 5194 are shown in Figure 6. We have again used *orthogonal distance regression* in Scipy (Virtanen et al. 2020) to fit a power-law to the B_{eq} and gas density data points. The scatters of the three correlations are shown in dashed lines in all the figures.

The measured best-fit power-law indices are 0.40 ± 0.02 , 0.49 ± 0.03 and 0.53 ± 0.02 (Table 9) for NGC 3627, NGC 4826 and NGC 5194, respectively. The mean of the power-law indices is 0.47 ± 0.05 .

4. EXTENDING THE SAMPLE WITH 5 GALAXIES FROM EXISTING GMRT OBSERVATIONS

As mentioned earlier, a study of B_{eq} and radio-FIR correlations for a sample of five large nearly face-on galaxies was carried out by Basu et al. (2012a,b); Basu & Roy (2013), using low-radio frequency observations at 0.33 and 1.4 GHz

Table 8. Best-fit parameters and the scatter of the correlation between magnetic fields and SFRSDs for the five galaxies in Basu et al. (2012a) (Sample 2). The data were fitted with a power law of the form $B=B_0(\Sigma_{\text{SFR}})^{\eta}$.

Name	Slope (η)	Intercept (B_0) ($\log(\mu\text{G})$)	Intercept (B_0) (μG)	Scatter
NGC 1097	0.27 ± 0.01	1.61 ± 0.01	41 ± 1.0	0.02
NGC 4736	0.32 ± 0.02	1.78 ± 0.05	60 ± 1.1	0.04
NGC 5055	0.27 ± 0.04	1.26 ± 0.02	18 ± 1.0	0.02
NGC 5236	0.38 ± 0.07	1.91 ± 0.02	81 ± 1.0	0.08
NGC 6946	0.25 ± 0.03	1.62 ± 0.05	42 ± 1.1	0.05

Table 9. Best-fit parameters and the scatter of the correlation between spatially-resolved magnetic fields and gas densities for the seven galaxies in Sample 3. Galaxies with an asterisk are from the sample of Basu et al. (2012a).

Name	Exponent	Scatter
NGC 3627	0.40 ± 0.02	0.03
NGC 4826	0.49 ± 0.03	0.05
NGC 5194	0.53 ± 0.02	0.06
NGC 4736*	0.44 ± 0.03	0.03
NGC 5055*	0.25 ± 0.02	0.02
NGC 5236*	0.40 ± 0.03	0.04
NGC 6946*	0.31 ± 0.03	0.04

at sub-kpc linear resolutions. In this paper, we expand our study of spatially-resolved correlations between magnetic fields, gas densities, and SFRSDs by including these five galaxies.

We refer readers to Basu et al. (2012a) for a detailed discussion of their sample, GMRT observations, data reduction procedures, and estimation of non-thermal spectral indices. It is to be noted that the modelling of the thermal free-free emission from these galaxies is performed in the same way as was done for our seven galaxies in Sample 1.

We have estimated the SFRSD maps of these five galaxies using $\text{H}\alpha$ data along with $24 \mu\text{m}$ IR data. We obtained $\text{H}\alpha$ maps of four of the galaxies, NGC 1097, NGC 4736, NGC 5055, and NGC 6946 from the ancillary data at the SINGS website¹ and obtained the $\text{H}\alpha$ map of NGC 5236 from 11HUGS (Kennicutt et al. 2008). We used $\text{H}\alpha$ and MIPS $24 \mu\text{m}$ data in combination to derive the SFRSD maps of these galaxies using the calibration from Leroy et al. (2012) (Equation 3, Section 2.2). To estimate the equipartition magnetic field strengths of these five galaxies, we have used the non-thermal radio maps at 0.33 and 1.4 GHz from Basu et al. (2012a). The correlations between equipartition magnetic fields and SFRSDs are shown in Figure 5 where, similar to the previous correlation studies, each point represents the logarithms of magnetic fields and SFRSD values that are averaged over the beam size. Similar to the previous correlations (Section 3.5), we used *orthogonal distance regression* in Scipy to fit a power law to the data. We have provided the best-fit parameters of the power-law fit in Table 8. The scatters of all five correlations (presented in Table 8) are shown in dashed lines in all the figures. We find a mean exponent of 0.30 ± 0.05 for the five galaxies where the exponent of individual galaxies varies from ≈ 0.25 to ≈ 0.38 .

We have computed maps of cold gas densities of four out of the five galaxies; NGC 4736, NGC 5055, NGC 5236 and NGC 6946, using the atomic and molecular gas surface density maps from Basu & Roy (2013). The assumed parameters are taken to be the same as described in Section 2.3. For the remaining galaxy, NGC 1097, we could not measure gas densities as there are no archival CO data available for the galaxy. Following the procedures of Section 3.5, we have also studied the spatially-resolved correlation between equipartition magnetic fields and gas densities for the four sample galaxies, which are shown in Figure 6. The best-fit parameters are presented in Table 9. The exponents of the individual galaxies vary between ≈ 0.25 to ≈ 0.44 where the mean exponent is found to be 0.35 ± 0.07 .

5. DISCUSSION

Understanding the relationship between the physical condition of the interstellar medium (ISM) and the star formation process is crucial to understand galaxy evolution. Gas and magnetic fields are key constituents of the

¹ <https://irsa.ipac.caltech.edu/data/SPITZER/SINGS/>

ISM and therefore it is important to study the interrelations between gas, magnetic fields, and SFRs. Though the Kennicutt–Schmidt relation, i.e. the relation between gas densities and SFRs, has been extensively studied at high spatial resolutions in various types of nearby galaxies (e.g. Onodera et al. 2010; Roychowdhury et al. 2015; Filho et al. 2016; Miettinen et al. 2017), similar high-resolution observations of how the magnetic fields are related to SFRs and gas densities are yet to be systematically investigated. Such observations are critical to understand the validity of several models that predict strong correlations between the magnetic fields and gas densities (e.g. Chandrasekhar & Fermi 1953; Fiedler & Mouschovias 1993; Cho & Vishniac 2000; Groves et al. 2003) as well as magnetic fields and SFRSDs (e.g. Niklas & Beck 1997; Schleicher & Beck 2013, 2016). Here, we have studied these correlations in a sample of twelve galaxies (Sample 3) at sub-kpc scales (see Sections 3.5, 3.6 & 4). To our knowledge, this is the first spatially resolved study of the above correlations in nearby large galaxies. In this section, we place these findings in the light of predictions made by various models and in the process attempt to provide physical insights into the interrelation between magnetic fields, gas densities, and star formation rates at sub-kpc scales.

5.1. Magnetic Fields and SFRSDs

Several Magneto-Hydrodynamical simulations find that galactic magnetic fields are amplified by gas turbulence in very short timescales (i.e. ~ 100 Myr) (e.g. Brandenburg & Subramanian 2005; Beresnyak 2012; Schober et al. 2012; Schleicher & Beck 2013; Bovino et al. 2013). The primary driver of gas-turbulence in the ISM of galaxies is supernova explosion (Bacchini et al. 2020), the rate of which is in turn directly coupled to the SFR in the galaxy. Therefore, it is expected that the star formation rates and the magnetic fields in a galaxy will be correlated. Indeed, using semi-analytical models, Schleicher & Beck (2013, 2016) found that in order to explain the radio-FIR correlation at sub-kpc scales, magnetic fields and SFRSDs, again at sub-kpc scales, must be related as $B \propto \Sigma_{\text{SFR}}^{1/3}$.

Studies in the literature on the correlation between magnetic fields and SFRSDs have focused on dwarf galaxies and those studies were carried out using galaxy-integrated magnetic fields and SFRSDs. As mentioned in Section 1, to our knowledge, there is only one published work of the spatially-resolved study of the correlation between magnetic fields and SFRSDs (Basu et al. 2017).

For the 12 galaxies in Sample 2 (Table 2), we find that the mean value of the power-law index of the correlation between B_{eq} and SFRSDs is 0.31 ± 0.06 , i.e. $B_{\text{eq}} \propto \Sigma_{\text{SFR}}^{0.31 \pm 0.06}$ (2), consistent (at $< 1\sigma$ error) with the model of Schleicher & Beck (2013, 2016). Thus, it appears that the semi-analytical models that are based on the amplification of magnetic fields due to supernova-driven gas turbulence work remarkably well for the pilot sample, in predicting the correlation between magnetic fields and SFRSDs down to sub-kpc scales.

We note that the power-law index for the correlation between B_{eq} and SFRSDs for NGC 4449 was found to be 0.18 ± 0.03 , significantly lower than for the remaining galaxies (Table 7) as well as lower than the model prediction of $B \propto \Sigma_{\text{SFR}}^{1/3}$ Schleicher & Beck (2013) (at $> 5\sigma$ significance). For the case of NGC 4449, the relatively flat spectral index values ($\alpha_{\text{nt}} \leq 0.55$) in $\approx 70\%$ of the galaxy meant that the magnetic field values could not be estimated reliably for a large part of the galaxy (see Section 2.1 and 3.5). This could lead to biases in the correlation and therefore, the low value of the power-law index for NGC 4449 should be taken with caution.

5.1.1. Intercept of the Correlation

According to the model proposed by Schleicher & Beck (2013), the intercept of the B - Σ_{SFR} correlation depends on several ISM parameters such as gas density (ρ_0), the fraction of turbulent kinetic energy converted into magnetic energy (f_{sat}), the injection rate of turbulent supernova energy (C) and the intercept of Kennicutt-Schmidt (KS) relation (C_1) (Equation 5).

$$B \sim \sqrt{f_{\text{sat}} 8\pi} \rho_0^{1/6} \left(\frac{C}{C_1}\right)^{1/3} \Sigma_{\text{SFR}}^{1/3}. \quad (6)$$

Schleicher & Beck (2013) predicted the intercept of the B - Σ_{SFR} correlation to be $\sim 26 \mu\text{G}$ assuming $\rho_0 = 10^{-24} \text{ g cm}^{-3}$ and $f_{\text{sat}} \sim 5$ percent. We have found an average intercept at $65 \pm 25 \mu\text{G}$ of the B_{eq} - Σ_{SFR} correlation of the 12 galaxies in sample 2 (see Table 7 & 8). Although the mean value is a factor of ≈ 2.5 higher than the value predicted by Schleicher & Beck (2013), this value is consistent with the predicted value, within the scatter (at $\approx 1.6\sigma$). Future follow-up studies, such as using our full survey (Sample 0 which consists of 46 galaxies), are required to draw statistically robust conclusions about the value of the intercept.

² The uncertainty quoted is the scatter of the measured value of η across the galaxies in Sample 2.

If the value of f_{sat} is indeed higher, this would imply a higher than assumed value of one or more of ρ_0 , C, and f_{sat} . The intercept is broadly insensitive to the assumed value of ρ_0 (Equation 6) and therefore, in order to explain a factor of ≈ 2.5 higher value of the intercept, the actual value ρ_0 has to be higher than the assumed value of 10^{-24} g cm $^{-3}$ by a factor of ≈ 240 ; such high gas densities are unphysical and are not observed in typical regions of a galaxy. The other possibility that the assumed value of the injection rate of turbulent supernova energy (C) is higher by a factor of ≈ 16 is also contrary to expectation; Basu et al. (2017) found that under reasonable conditions the value of C can be higher by at most a factor of 1.4. Therefore, f_{sat} must be higher than 0.05 to explain a significantly higher value of the intercept. An understanding of how galaxies can achieve such efficient amplification of magnetic fields with f_{sat} much greater than 5% requires detailed MHD simulations. We note that Basu et al. (2017) found that the value of the intercept for B- Σ_{SFR} for the dwarf galaxy IC 10 is 51 μ G, similar to our findings of a higher than predicted value of the intercept.

5.2. Magnetic Fields and Gas

Magnetic fields and gas are expected to be correlated as $B \propto \sqrt{\rho_{gas}}$ (e.g. Chandrasekhar & Fermi 1953; Groves et al. 2003). We find that equipartition magnetic fields are correlated with gas densities for the seven galaxies (Sample 3) with an average power-law index, $k=0.40\pm 0.09$ (see Section 3.6 & 4)³. This value of k is consistent with the numerical simulations that predict $k \approx 0.4-0.6$ and also consistent with the theories that predict $B \propto \rho_{gas}^{0.5}$. The power-law index of the correlation between B_{eq} and gas densities is found to be 0.25 ± 0.02 and 0.31 ± 0.03 for NGC 5055 and NGC 6946 respectively, significantly lower than the model predictions and as compared to the other galaxies in Sample 3. A lower value of k could mean that either the efficiency of the amplification of the magnetic field is less or that the magnetic field strengths derived assuming the ‘‘minimum energy condition’’ are underestimated (Dumas et al. 2011). Strong synchrotron or inverse Compton losses of cosmic-ray electrons could suppress the radio synchrotron emission which would then cause the equipartition magnetic fields to be underestimated.

5.2.1. Magnetic Fields, Gas Densities and the Radio-FIR Correlations

Energy equipartition between the magnetic field (B) and the gas density (ρ_{gas}), and between magnetic fields and cosmic ray particles implies that the non-thermal emission is related to the gas density as $I_{nt} \propto \rho_{gas}^{k(3+\alpha_{nt})}$ where k is the power-law index relating magnetic fields and gas densities ($B_{eq} \propto \rho_{gas}^k$) (Niklas & Beck 1997). Further, the Kennicutt-Schmidt law and the radio-FIR correlation imply that I_{nt} is related to gas densities as (1) $I_{nt} \propto \rho_{gas}^{m(n+1)}$ for optically thin dust to UV photons and (2) $I_{nt} \propto \rho_{gas}^{mn}$ for optically thick dust to UV photons, where m is the power-law index of the radio-FIR correlation and n is the power-law index of the Kennicutt-Schmidt law. Therefore, we can obtain the following relation between the power-law index of all four correlations (Dumas et al. 2011):

$$k = \frac{(n+1)m}{3+\alpha_{nt}}; \text{Optically thin dust} \quad (7)$$

$$k = \frac{nm}{3+\alpha_{nt}}; \text{Optically thick dust} \quad (8)$$

We can use the above equations to indirectly estimate the power-law index, k , of the correlation between magnetic fields and gas densities. For the three galaxies, NGC 3627, NGC 4826, and NGC 5194 (Roy & Manna 2021), we have estimated gas densities using CO and HI observations. Now we can compare the direct measurement of k with an indirect estimate of k using Equations 7 and 8; this will provide additional information on the validity of both the minimum energy conditions that were assumed between magnetic fields and the gas densities as well as the magnetic fields and cosmic ray particles. For the galaxies from Basu et al. (2012a), this study was already presented and discussed in Basu et al. (2012b).

We have estimated k for all the seven sample galaxies from Roy & Manna (2021) (Sample 1), using the assumption of optically thin dust to UV photons, using (i) the slope of radio-FIR correlation (m) as derived in Roy & Manna (2021), (ii) the measured galaxy-averaged spectral index (α_{nt}) from Roy & Manna (2021), and (iii) a Kennicutt-Schmidt power-law index of 1.4 ± 0.15 (Kennicutt 1998b).

Table 10 provides the relevant values as well as estimated values of k derived using the measured value of m using radio emission at both 0.33 and 1.4 GHz. For two of the galaxies, NGC 3627 & NGC 5194, the value of k estimated

³ The uncertainty quoted is the scatter of the measured value of k across the galaxies in Sample 3.

Table 10. Power law index (k) of the relation between magnetic fields and gas densities ($B \propto \rho^k$) of galaxies in Sample 1, indirectly estimated using the slope of radio-FIR correlation (m) and the slope of the Kennicutt–Schmidt law. See Section 5.2.1 for a discussion on these.

Name	m		α_{nt}	k (Optically thin)	
	0.33 GHz	1.4 GHz		0.33 GHz	1.4 GHz
NGC 2683	0.54±0.06	0.91±0.07	-0.84±0.08	0.33 ± 0.04	0.57 ± 0.06
NGC 3627	0.55±0.03	0.85±0.13	-1.10±0.07	0.32 ± 0.03	0.50 ± 0.08
NGC 4096	0.74±0.05	0.90±0.04	-0.78±0.06	0.47 ± 0.04	0.57 ± 0.05
NGC 4449	0.77±0.05	0.65±0.04	-0.48±0.06	0.53 ± 0.05	0.45 ± 0.04
NGC 4490	0.68±0.02	0.75±0.02	-0.59±0.07	0.45 ± 0.03	0.50 ± 0.04
NGC 4826	1.39±0.1	1.47±0.08	-0.49±0.06	0.95 ± 0.09	1.00 ± 0.09
NGC 5194(arm)	0.50±0.05	0.65±0.04	-0.63±0.05	0.33± 0.04	0.43 ± 0.04
NGC 5194(interarm)	0.73±0.11	1.03±0.05	-0.85±0.10	0.46± 0.08	0.64 ± 0.05

using Equation 7 is comparable to the direct measurement of k . This broadly validates the assumption of energy equipartition between magnetic fields and cosmic ray particles in these two galaxies.

For the optically thin case, the mean of indirectly-estimated k values of the sample of seven galaxies are 0.59 ± 0.16 and 0.53 ± 0.19 at 1.4 and 0.33 GHz, respectively. However, this includes the galaxy NGC 4826, which shows an anomalously high value of $k=1.0$ and 0.95 derived at 1.4 and 0.33 GHz, respectively. Excluding this galaxy from the mean calculation, we find that $k=0.52 \pm 0.04$ and 0.47 ± 0.09 at 1.4 and 0.33 GHz, respectively. Remarkably, for all the galaxies except NGC 4826, the k value at 1.4 GHz, for the optically thin case, is consistent with 0.5 within error bars. Thus, the indirectly estimated values of k are consistent with equipartition between magnetic fields and gas energy densities (Chandrasekhar & Fermi 1953; Fiedler & Mouschovias 1993; Cho & Vishniac 2000; Groves et al. 2003). This is similar to the findings of Niklas & Beck (1997) for their sample of 43 galaxies and Basu et al. (2012b) for their sample of four galaxies.

The value of k derived for NGC 4826, for the optically thin case, is a consequence of the anomalously high value of the power-law index of the radio-FIR correlation (≈ 1.39 and ≈ 1.47 for 0.33 and 1.4 GHz respectively, Table 10) which is different from the other six galaxies in the sample. NGC 4826 has been classified as a Seyfert 2 galaxy in the past (Malkan et al. 2017) and therefore the emission from the core contributes to the observed power-law index of the radio-FIR correlation (Roy & Manna 2021). It is likely that the significant contribution of the AGN to the radio emission makes the estimate of k for NGC 4826 unreliable.

6. SUMMARY

1. We made spatially resolved maps of equipartition magnetic fields in seven galaxies (Sample 1): NGC 2683, NGC 3627, NGC 4096, NGC 4449, NGC 4490, NGC 4826, and NGC 5194 and find that the magnetic fields are strongest near the central region and go down by a factor of ~ 2 at the edge of the magnetic field maps.
2. We have used the tightness of the spatially-resolved radio-FIR correlations to verify the validity of the equipartition condition between magnetic fields and cosmic ray particles for the sample galaxies. We find that the magnetic field values may deviate from the equipartition values by $\sim 25\%$.
3. We have estimated spatially resolved maps of SFRSDs of the galaxies in Sample 1 using FUV+24 μ m, H α +24 μ m, and 1.4 GHz data. Azimuthally averaged SFRSDs drop by a factor of 6 to 8 at the edge of the galaxies, where SFRSD values are 5 times the rms of the maps.
4. We also included five additional galaxies: NGC 1097, NGC 4736, NGC 5055, NGC 5236, and NGC 6946 from previous GMRT observations of Basu et al. (2012a) and estimated their equipartition magnetic field, SFRSD and gas density maps.
5. We studied the spatial correlation between magnetic fields and star formation rates at < 1 kpc resolution for the 12 galaxies (Sample 2) and find that magnetic field strengths and SFRSDs are correlated with an average power-law index of 0.31 ± 0.06 . This result is in remarkable agreement (at $< 1\sigma$ error) with semi-analytical model predictions of $B \propto \Sigma_{\text{SFR}}^{1/3}$ (Schleicher & Beck 2013, 2016).

6. We measure an average intercept of $\approx 65 \mu\text{G}$ from the B - Σ_{SFR} correlations of our galaxies in Sample 2. This is higher than the predictions of [Schleicher & Beck \(2013\)](#) by a factor of ≈ 2.5 , and, if confirmed with a larger sample, would imply a significantly higher efficiency of magnetic field amplification than what is typically assumed.
7. We used spatially resolved gas density maps for seven (Sample 3) of the 12 galaxies, for which archival CO data was available, to find that magnetic fields are correlated with gas densities as $B \propto \rho_{\text{gas}}^{0.40 \pm 0.09}$. This result is consistent with numerical simulations that predict $k \approx 0.4$ – 0.6 and broadly consistent (within ≈ 1 sigma uncertainty) with theories that predict $B \propto \rho_{\text{gas}}^{0.5}$.
8. We have indirectly estimated the power-law index (k) of the correlation between the magnetic fields and the gas densities using the slope of the radio-FIR correlation, the slope of the Kennicutt-Schmidt law, and the non-thermal spectral index. The mean value of k , for optically thin dust, was found to be 0.52 ± 0.04 and 0.47 ± 0.09 at 1.4 and 0.33 GHz respectively for the six galaxies in Sample 1, with NGC 4826 excluded due to its high value of k . This is consistent with the equipartition between magnetic fields and gas. The anomalously high values of k (1.0 and 0.95 at 1.4 and 0.33 GHz respectively) for NGC 4826 are possibly due to the contribution of the central AGN to the radio emission.

We have started to follow up these pilot study results with a survey of a much larger sample of galaxies (Sample 0, Table 2). For this, we have already observed another 24 galaxies using the upgraded GMRT (uGMRT), a Square Kilometer Array (SKA) pathfinder facility. Sensitivities of the images from these uGMRT observations are significantly better (≈ 3 times) than those of the observations presented here and the result will be part of a future publication. In addition, SKA precursors such as the MeerKAT will also provide very deep images of the diffuse radio-continuum emission around nearby galaxies. Eventually, the dramatic increase in sensitivity and \sim arc-sec resolution of the SKA has the potential to significantly advance our understanding of magnetic fields in nearby galaxies. For example, the SKA is expected to provide sensitive images of polarised synchrotron emission from nearby galaxies at a few GHz frequencies which would provide information on the large-scale ordered fields on the plane of the sky (e.g. [Johnston-Hollitt et al. 2015](#)). Further, polarised emission from nearby galaxies at $< \sim 1$ GHz, where significant depolarisations take place, could be modelled through Faraday tomography (e.g. [Heald et al. 2015](#)). A combination of the two approaches could eventually allow us to infer the three-dimensional structure of the magnetic fields in nearby galaxies. SKA observations will also provide detailed images of star formation with resolutions of tens of parsecs. These will help to identify any dependence of SFR and IMF on galaxy type, evolution and environment within the local volume ([Beswick et al. 2015](#)).

1 We would like to thank Aditya Chowdhury for his help at various stages of this research. We thank Yogesh Wadadkar,
2 Preeti Kharb, and Dipanjan Mitra for reading the manuscript and providing useful comments. Aritra Basu provided
3 their earlier published images and also suggested checking the B vs SFRSD relation for our sample galaxies. We
4 thank him for the above. We also thank the anonymous referee whose comments helped significantly improve the
5 presentation of the paper. We thank the staff of GMRT that allowed these observations to be made. GMRT is run by
6 National Centre for Radio Astrophysics of the Tata Institute of fundamental research. We acknowledge the support
7 of the Department of Atomic Energy, Government of India, under project no. 12-R&D-TFR-5.02-0700.

REFERENCES

- | | |
|---|--|
| <p>Adebahr, B., Krause, M., Klein, U., et al. 2013, <i>A&A</i>, 555, A23, doi: 10.1051/0004-6361/201220226</p> <p>Bacchini, C., Fraternali, F., Iorio, G., et al. 2020, <i>A&A</i>, 641, A70, doi: 10.1051/0004-6361/202038223</p> <p>Basu, A., Mitra, D., Wadadkar, Y., & Ishwara-Chandra, C. H. 2012a, <i>MNRAS</i>, 419, 1136, doi: 10.1111/j.1365-2966.2011.19764.x</p> <p>Basu, A., & Roy, S. 2013, <i>MNRAS</i>, 433, 1675, doi: 10.1093/mnras/stt845</p> | <p>Basu, A., Roy, S., & Mitra, D. 2012b, <i>ApJ</i>, 756, 141, doi: 10.1088/0004-637X/756/2/141</p> <p>Basu, A., Roychowdhury, S., Heesen, V., et al. 2017, <i>MNRAS</i>, 471, 337, doi: 10.1093/mnras/stx1567</p> <p>Batchelor, G. K. 1950, <i>Proceedings of the Royal Society of London Series A</i>, 201, 405, doi: 10.1098/rspa.1950.0069</p> <p>Beck, R., Brandenburg, A., Moss, D., Shukurov, A., & Sokoloff, D. 1996, <i>ARA&A</i>, 34, 155, doi: 10.1146/annurev.astro.34.1.155</p> |
|---|--|

- Beck, R., & Krause, M. 2005, *Astronomische Nachrichten*, 326, 414, doi: [10.1002/asna.200510366](https://doi.org/10.1002/asna.200510366)
- Bell, E. F. 2003, *ApJ*, 586, 794, doi: [10.1086/367829](https://doi.org/10.1086/367829)
- Beresnyak, A. 2012, *PhRvL*, 108, 035002, doi: [10.1103/PhysRevLett.108.035002](https://doi.org/10.1103/PhysRevLett.108.035002)
- Beswick, R., Brinks, E., Perez-Torres, M., et al. 2015, in *Advancing Astrophysics with the Square Kilometre Array (AASKA14)*, 70. <https://arxiv.org/abs/1412.5810>
- Bianchi, L., Shiao, B., & Thilker, D. 2017, *ApJS*, 230, 24, doi: [10.3847/1538-4365/aa7053](https://doi.org/10.3847/1538-4365/aa7053)
- Bolatto, A. D., Wolfire, M., & Leroy, A. K. 2013, *ARA&A*, 51, 207, doi: [10.1146/annurev-astro-082812-140944](https://doi.org/10.1146/annurev-astro-082812-140944)
- Bovino, S., Schleicher, D. R. G., & Schober, J. 2013, *New Journal of Physics*, 15, 013055, doi: [10.1088/1367-2630/15/1/013055](https://doi.org/10.1088/1367-2630/15/1/013055)
- Brandenburg, A., & Subramanian, K. 2005, *PhR*, 417, 1, doi: [10.1016/j.physrep.2005.06.005](https://doi.org/10.1016/j.physrep.2005.06.005)
- Buat, V. 1992, *A&A*, 264, 444
- Chandrasekhar, S., & Fermi, E. 1953, *ApJ*, 118, 113, doi: [10.1086/145731](https://doi.org/10.1086/145731)
- Cho, J., & Vishniac, E. T. 2000, *ApJ*, 539, 273, doi: [10.1086/309213](https://doi.org/10.1086/309213)
- Chyży, K. T., Beck, R., Kohle, S., Klein, U., & Urbanik, M. 2000, *A&A*, 355, 128. <https://arxiv.org/abs/astro-ph/0001205>
- Chyży, K. T., & Buta, R. J. 2008, *ApJL*, 677, L17, doi: [10.1086/587958](https://doi.org/10.1086/587958)
- Chyży, K. T., Weżgowiec, M., Beck, R., & Bomans, D. J. 2011, *A&A*, 529, A94, doi: [10.1051/0004-6361/201015393](https://doi.org/10.1051/0004-6361/201015393)
- Clemens, M. S., Alexander, P., & Green, D. A. 1999, *MNRAS*, 307, 481, doi: [10.1046/j.1365-8711.1999.02594.x](https://doi.org/10.1046/j.1365-8711.1999.02594.x)
- Cortese, L., Boselli, A., Franzetti, P., et al. 2008, *MNRAS*, 386, 1157, doi: [10.1111/j.1365-2966.2008.13118.x](https://doi.org/10.1111/j.1365-2966.2008.13118.x)
- Crutcher, R. M. 1999, in *Science with the Atacama Large Millimeter Array (ALMA)*, 12
- da Silva, R. L., Fumagalli, M., & Krumholz, M. R. 2014, *MNRAS*, 444, 3275, doi: [10.1093/mnras/stu1688](https://doi.org/10.1093/mnras/stu1688)
- Dale, D. A., Cohen, S. A., Johnson, L. C., et al. 2009, *ApJ*, 703, 517, doi: [10.1088/0004-637X/703/1/517](https://doi.org/10.1088/0004-637X/703/1/517)
- Dumas, G., Schinnerer, E., Tabatabaei, F. S., et al. 2011, *AJ*, 141, 41, doi: [10.1088/0004-6256/141/2/41](https://doi.org/10.1088/0004-6256/141/2/41)
- Elmegreen, B. G. 1981, *ApJ*, 243, 512, doi: [10.1086/158616](https://doi.org/10.1086/158616)
- Fiedler, R. A., & Mouschovias, T. C. 1993, *ApJ*, 415, 680, doi: [10.1086/173193](https://doi.org/10.1086/173193)
- Filho, M. E., Sánchez Almeida, J., Amorín, R., et al. 2016, *ApJ*, 820, 109, doi: [10.3847/0004-637X/820/2/109](https://doi.org/10.3847/0004-637X/820/2/109)
- Fletcher, A., Beck, R., Shukurov, A., Berkhuijsen, E. M., & Horellou, C. 2011, *MNRAS*, 412, 2396, doi: [10.1111/j.1365-2966.2010.18065.x](https://doi.org/10.1111/j.1365-2966.2010.18065.x)
- Groves, B. A., Cho, J., Dopita, M., & Lazarian, A. 2003, *PASA*, 20, 252, doi: [10.1071/AS03016](https://doi.org/10.1071/AS03016)
- Heald, G., Beck, R., de Blok, W. J. G., et al. 2015, in *Advancing Astrophysics with the Square Kilometre Array (AASKA14)*, 106. <https://arxiv.org/abs/1501.00408>
- Heesen, V., Beck, R., Krause, M., & Dettmar, R. J. 2009, *A&A*, 494, 563, doi: [10.1051/0004-6361:200810543](https://doi.org/10.1051/0004-6361:200810543)
- Heesen, V., Brinks, E., Leroy, A. K., et al. 2014, *AJ*, 147, 103, doi: [10.1088/0004-6256/147/5/103](https://doi.org/10.1088/0004-6256/147/5/103)
- Hummel, E. 1986, *A&A*, 160, L4
- Irwin, J., Beck, R., Benjamin, R. A., et al. 2012, *AJ*, 144, 44, doi: [10.1088/0004-6256/144/2/44](https://doi.org/10.1088/0004-6256/144/2/44)
- Johnston-Hollitt, M., Govoni, F., Beck, R., et al. 2015, in *Advancing Astrophysics with the Square Kilometre Array (AASKA14)*, 92. <https://arxiv.org/abs/1506.00808>
- Jurusik, W., Drzazga, R. T., Jableka, M., et al. 2014, *A&A*, 567, A134, doi: [10.1051/0004-6361/201323060](https://doi.org/10.1051/0004-6361/201323060)
- Kazes, I., Troland, T. H., & Crutcher, R. M. 1991, *A&A*, 245, L17
- Kennicutt, Robert C., J. 1998a, *ApJ*, 498, 541, doi: [10.1086/305588](https://doi.org/10.1086/305588)
- . 1998b, *ARA&A*, 36, 189, doi: [10.1146/annurev.astro.36.1.189](https://doi.org/10.1146/annurev.astro.36.1.189)
- Kennicutt, Robert C., J., Lee, J. C., Funes, J. G., et al. 2008, *ApJS*, 178, 247, doi: [10.1086/590058](https://doi.org/10.1086/590058)
- Kennicutt, Robert C., J., Armus, L., Bendo, G., et al. 2003, *PASP*, 115, 928, doi: [10.1086/376941](https://doi.org/10.1086/376941)
- Kennicutt, Robert C., J., Calzetti, D., Walter, F., et al. 2007, *ApJ*, 671, 333, doi: [10.1086/522300](https://doi.org/10.1086/522300)
- Kennicutt, R. C., & Evans, N. J. 2012a, *ARA&A*, 50, 531, doi: [10.1146/annurev-astro-081811-125610](https://doi.org/10.1146/annurev-astro-081811-125610)
- . 2012b, *ARA&A*, 50, 531, doi: [10.1146/annurev-astro-081811-125610](https://doi.org/10.1146/annurev-astro-081811-125610)
- Kierdorf, M., Mao, S. A., Beck, R., et al. 2020, *A&A*, 642, A118, doi: [10.1051/0004-6361/202037847](https://doi.org/10.1051/0004-6361/202037847)
- Kim, J., Balsara, D., & Mac Low, M.-M. 2001, *Journal of Korean Astronomical Society*, 34, 333, doi: [10.5303/JKAS.2001.34.4.333](https://doi.org/10.5303/JKAS.2001.34.4.333)
- Krause, M. 2009, in *Revista Mexicana de Astronomía y Astrofísica Conference Series, Vol. 36, Revista Mexicana de Astronomía y Astrofísica Conference Series*, 25–29. <https://arxiv.org/abs/0806.2060>
- Krause, M., Wielebinski, R., & Dumke, M. 2006, *A&A*, 448, 133, doi: [10.1051/0004-6361:20053789](https://doi.org/10.1051/0004-6361:20053789)
- Krause, M., Irwin, J., Schmidt, P., et al. 2020, *A&A*, 639, A112, doi: [10.1051/0004-6361/202037780](https://doi.org/10.1051/0004-6361/202037780)
- Kroupa, P. 2001, *MNRAS*, 322, 231, doi: [10.1046/j.1365-8711.2001.04022.x](https://doi.org/10.1046/j.1365-8711.2001.04022.x)

- Kulsrud, R. M., & Zweibel, E. G. 2008, Reports on Progress in Physics, 71, 046901, doi: [10.1088/0034-4885/71/4/046901](https://doi.org/10.1088/0034-4885/71/4/046901)
- Leroy, A. K., Walter, F., Bigiel, F., et al. 2009, AJ, 137, 4670, doi: [10.1088/0004-6256/137/6/4670](https://doi.org/10.1088/0004-6256/137/6/4670)
- Leroy, A. K., Bigiel, F., de Blok, W. J. G., et al. 2012, AJ, 144, 3, doi: [10.1088/0004-6256/144/1/3](https://doi.org/10.1088/0004-6256/144/1/3)
- Longair, M. S. 2011, High Energy Astrophysics
- Malkan, M. A., Jensen, L. D., Rodriguez, D. R., Spinoglio, L., & Rush, B. 2017, ApJ, 846, 102, doi: [10.3847/1538-4357/aa8302](https://doi.org/10.3847/1538-4357/aa8302)
- Meurer, G. R., Heckman, T. M., & Calzetti, D. 1999, ApJ, 521, 64, doi: [10.1086/307523](https://doi.org/10.1086/307523)
- Meurer, G. R., Heckman, T. M., Leitherer, C., et al. 1995, AJ, 110, 2665, doi: [10.1086/117721](https://doi.org/10.1086/117721)
- Miettinen, O., Delvecchio, I., Smolčić, V., et al. 2017, A&A, 602, L9, doi: [10.1051/0004-6361/201731157](https://doi.org/10.1051/0004-6361/201731157)
- Miley, G. 1980, ARA&A, 18, 165, doi: [10.1146/annurev.aa.18.090180.001121](https://doi.org/10.1146/annurev.aa.18.090180.001121)
- Moss, D., & Shukurov, A. 1996, MNRAS, 279, 229, doi: [10.1093/mnras/279.1.229](https://doi.org/10.1093/mnras/279.1.229)
- Murphy, E. J., Helou, G., Kenney, J. D. P., Armus, L., & Braun, R. 2008, ApJ, 678, 828, doi: [10.1086/587123](https://doi.org/10.1086/587123)
- Murphy, E. J., Braun, R., Helou, G., et al. 2006a, ApJ, 638, 157, doi: [10.1086/498636](https://doi.org/10.1086/498636)
- Murphy, E. J., Helou, G., Braun, R., et al. 2006b, ApJL, 651, L111, doi: [10.1086/509722](https://doi.org/10.1086/509722)
- Murphy, E. J., Condon, J. J., Schinnerer, E., et al. 2011, ApJ, 737, 67, doi: [10.1088/0004-637X/737/2/67](https://doi.org/10.1088/0004-637X/737/2/67)
- Nikiel-Wroczyński, B., Jamrozy, M., Soida, M., Urbanik, M., & Knapik, J. 2016, MNRAS, 459, 683, doi: [10.1093/mnras/stw414](https://doi.org/10.1093/mnras/stw414)
- Niklas, S., & Beck, R. 1997, A&A, 320, 54
- Onodera, S., Kuno, N., Tosaki, T., et al. 2010, ApJL, 722, L127, doi: [10.1088/2041-8205/722/2/L127](https://doi.org/10.1088/2041-8205/722/2/L127)
- Pacholczyk, A. G. 1970, Radio astrophysics. Nonthermal processes in galactic and extragalactic sources
- Price, D. J., & Bate, M. R. 2008, MNRAS, 385, 1820, doi: [10.1111/j.1365-2966.2008.12976.x](https://doi.org/10.1111/j.1365-2966.2008.12976.x)
- Regan, M. W., Thornley, M. D., Helfer, T. T., et al. 2001, ApJ, 561, 218, doi: [10.1086/323221](https://doi.org/10.1086/323221)
- Robishaw, T., Quataert, E., & Heiles, C. 2008, ApJ, 680, 981, doi: [10.1086/588031](https://doi.org/10.1086/588031)
- Roy, S., & Manna, S. 2021, MNRAS, 507, 4734, doi: [10.1093/mnras/stab2441](https://doi.org/10.1093/mnras/stab2441)
- Roychowdhury, S., Huang, M.-L., Kauffmann, G., Wang, J., & Chengalur, J. N. 2015, MNRAS, 449, 3700, doi: [10.1093/mnras/stv515](https://doi.org/10.1093/mnras/stv515)
- Sarazin, C. L. 1999, ApJ, 520, 529, doi: [10.1086/307501](https://doi.org/10.1086/307501)
- Sarma, A. P., Momjian, E., Troland, T. H., & Crutcher, R. M. 2005, AJ, 130, 2566, doi: [10.1086/497637](https://doi.org/10.1086/497637)
- Schleicher, D. R. G., & Beck, R. 2013, A&A, 556, A142, doi: [10.1051/0004-6361/201321707](https://doi.org/10.1051/0004-6361/201321707)
- . 2016, A&A, 593, A77, doi: [10.1051/0004-6361/201628843](https://doi.org/10.1051/0004-6361/201628843)
- Schober, J., Schleicher, D., Federrath, C., et al. 2012, ApJ, 754, 99, doi: [10.1088/0004-637X/754/2/99](https://doi.org/10.1088/0004-637X/754/2/99)
- Shukurov, A., Sokoloff, D., Subramanian, K., & Brandenburg, A. 2006, A&A, 448, L33, doi: [10.1051/0004-6361:200600011](https://doi.org/10.1051/0004-6361:200600011)
- Soida, M., Urbanik, M., Beck, R., Wielebinski, R., & Balkowski, C. 2001, A&A, 378, 40, doi: [10.1051/0004-6361:20011185](https://doi.org/10.1051/0004-6361:20011185)
- Sokoloff, D. D., Bykov, A. A., Shukurov, A., et al. 1998, MNRAS, 299, 189, doi: [10.1046/j.1365-8711.1998.01782.x](https://doi.org/10.1046/j.1365-8711.1998.01782.x)
- Tabatabaei, F. S., Berkhuijsen, E. M., Frick, P., Beck, R., & Schinnerer, E. 2013, A&A, 557, A129, doi: [10.1051/0004-6361/201218909](https://doi.org/10.1051/0004-6361/201218909)
- Thompson, T. A., Quataert, E., Waxman, E., Murray, N., & Martin, C. L. 2006, ApJ, 645, 186, doi: [10.1086/504035](https://doi.org/10.1086/504035)
- Van Loo, S., Tan, J. C., & Falle, S. A. E. G. 2015, ApJL, 800, L11, doi: [10.1088/2041-8205/800/1/L11](https://doi.org/10.1088/2041-8205/800/1/L11)
- Vargas, C. J., Mora-Partiarroyo, S. C., Schmidt, P., et al. 2018, ApJ, 853, 128, doi: [10.3847/1538-4357/aaa47f](https://doi.org/10.3847/1538-4357/aaa47f)
- Virtanen, P., Gommers, R., Oliphant, T. E., et al. 2020, Nature Methods, 17, 261, doi: [10.1038/s41592-019-0686-2](https://doi.org/10.1038/s41592-019-0686-2)
- Walter, F., Brinks, E., de Blok, W. J. G., et al. 2008, AJ, 136, 2563, doi: [10.1088/0004-6256/136/6/2563](https://doi.org/10.1088/0004-6256/136/6/2563)
- Watanabe, Y., Sorai, K., Kuno, N., & Habe, A. 2011, MNRAS, 411, 1409, doi: [10.1111/j.1365-2966.2010.17746.x](https://doi.org/10.1111/j.1365-2966.2010.17746.x)
- Wiegert, T., Irwin, J., Miskolczy, A., et al. 2015, AJ, 150, 81, doi: [10.1088/0004-6256/150/3/81](https://doi.org/10.1088/0004-6256/150/3/81)
- Yun, M. S., Reddy, N. A., & Condon, J. J. 2001, ApJ, 554, 803, doi: [10.1086/323145](https://doi.org/10.1086/323145)

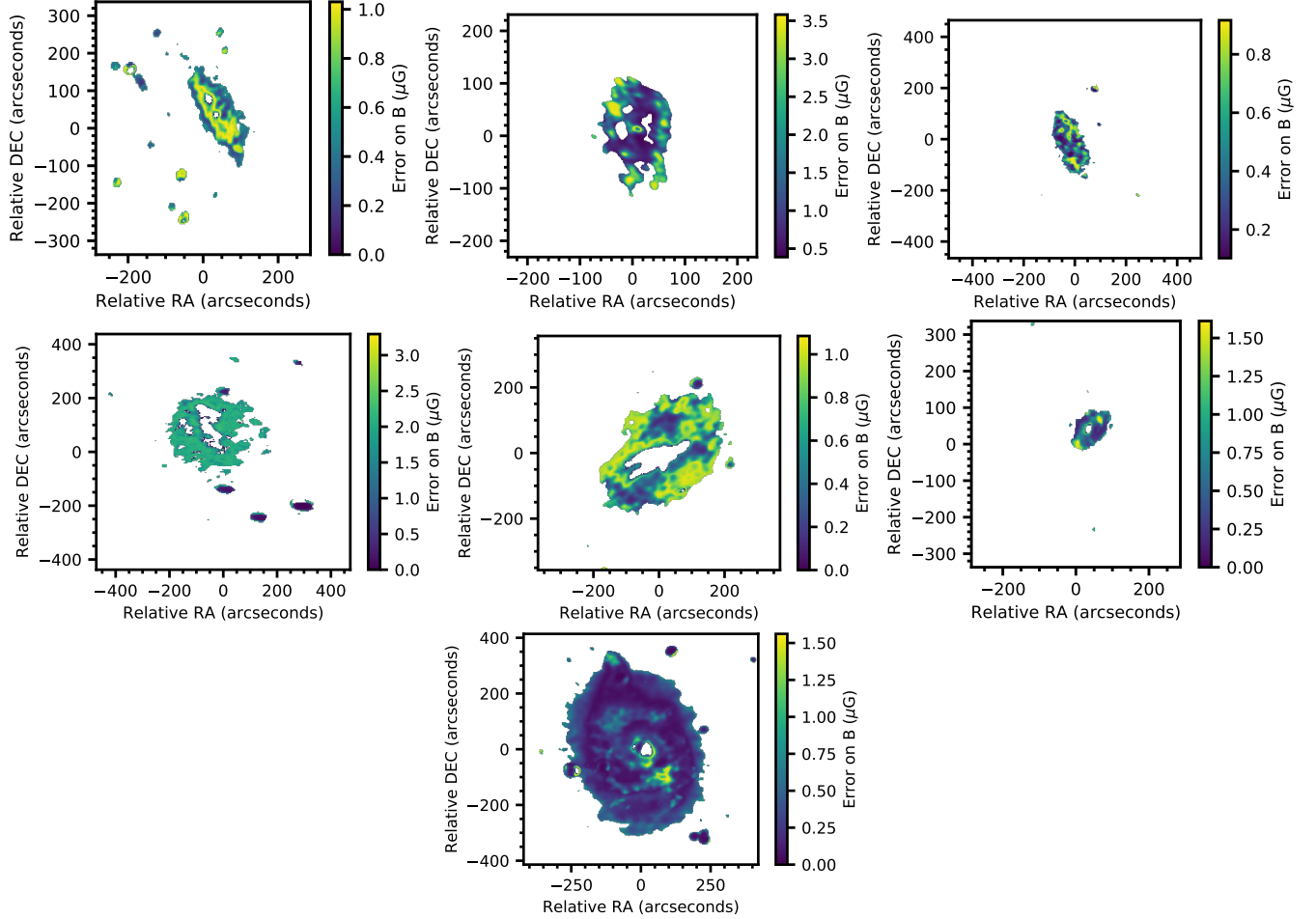


Figure 7. The magnetic field uncertainty maps (in μG) of NGC 2683 (top left), NGC 3627 (top centre), NGC 4096 (top right), NGC 4449 (middle left), NGC 4490 (middle centre), NGC 4826 (middle right) and NGC 5194 (bottom) (Sample 1), shown in colour scale. Blanked regions (in white colour) in the centre of each galaxy correspond to regions with spectral index values ≤ 0.55 .

APPENDIX

A. MAGNETIC FIELD UNCERTAINTY MAPS

We present here (Figure 7) magnetic field uncertainty maps of the galaxies in Sample 1, generated using the procedure described in Section 2.1.1.

B. STAR FORMATION RATE SURFACE DENSITY MAPS

We show SFRSD maps of the seven galaxies (Sample 1) in Figures 8 and 9, where SFRSDs estimated using 1.4 GHz and FUV+24 μm emission are shown in contours and colors, respectively. In Figures 10 and 11, we have also shown the SFRSD maps estimated using H α +24 μm and 1.4GHz data in colors and contours, respectively. The SFRSD maps of each galaxy in Figures 8, 9, 10, and 11 have been shown in the same color scale and contours.

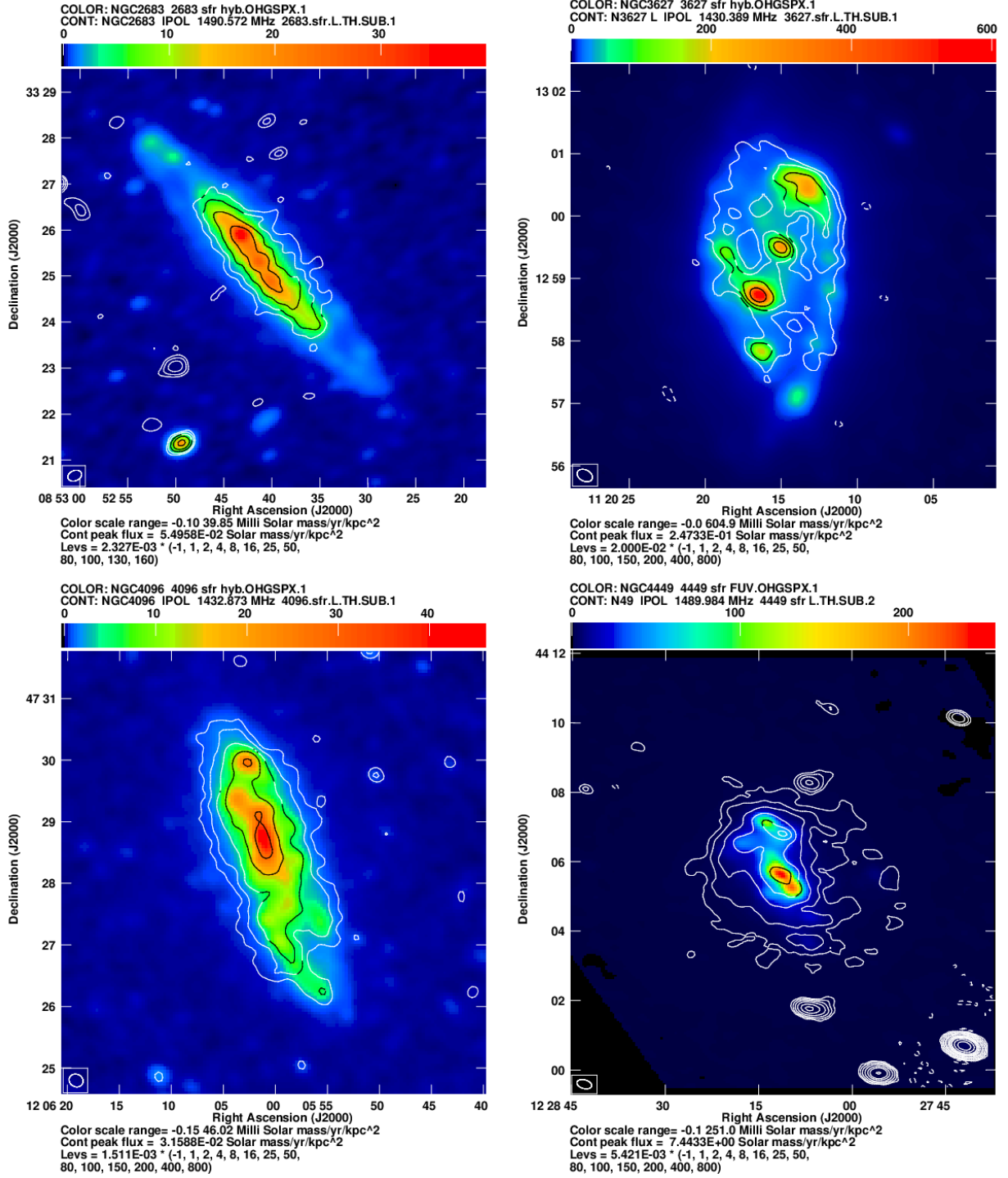


Figure 8. SFRSD ($M_{\odot}\text{yr}^{-1}\text{kpc}^{-2}$) maps of NGC 2683, NGC 3627, NGC 4449 and NGC 4096 (clockwise from top left) (Sample 1). SFRSDs estimated using 1.4 GHz radio and FUV+ $24\mu\text{m}$ emission are shown in contours and colors, respectively. Contour levels are listed below each panel of the figure. The circle in the bottom-left corner of the images indicates the angular resolution of the maps.

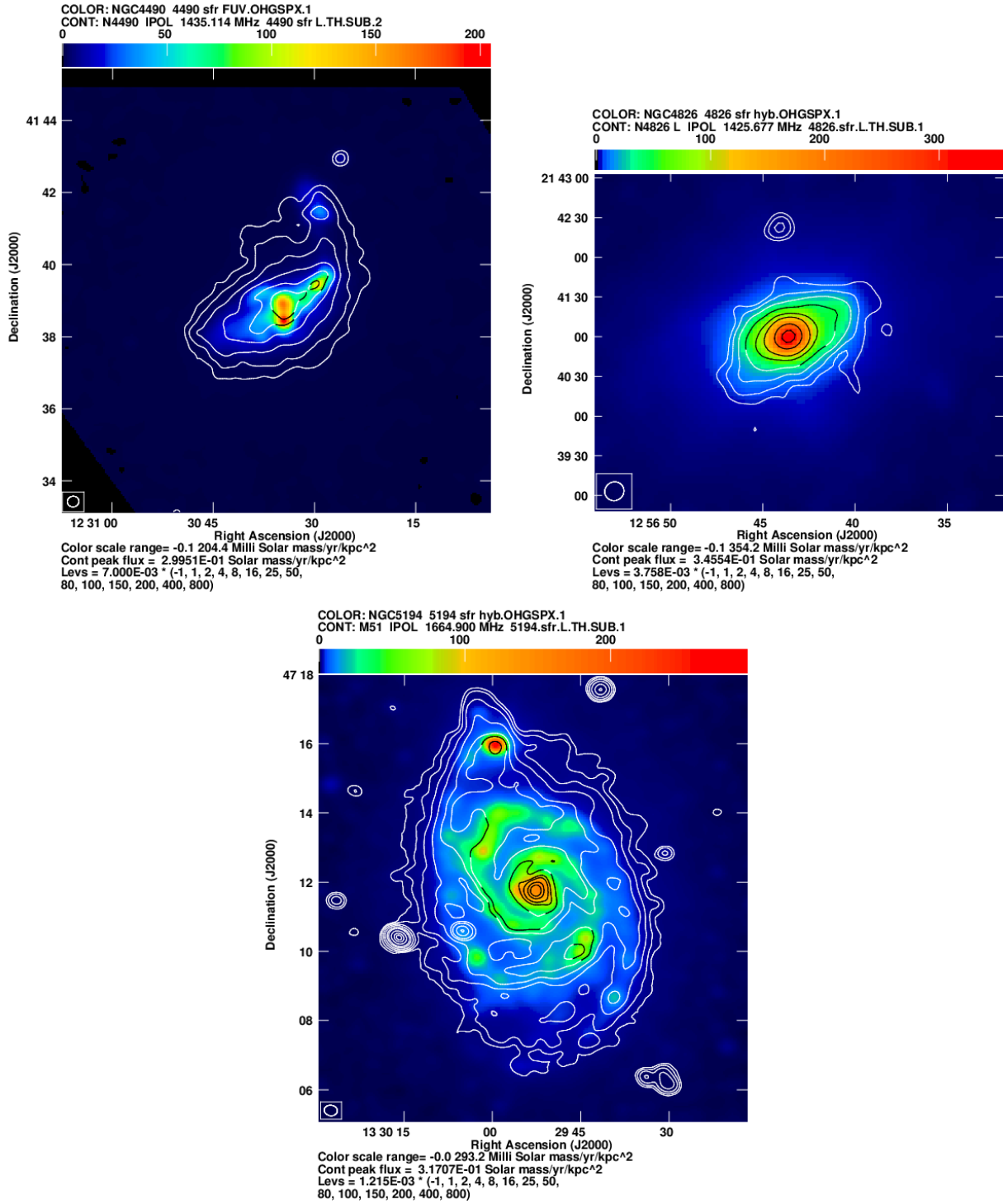


Figure 9. SFRSD ($M_{\odot}\text{yr}^{-1}\text{kpc}^{-2}$) maps of NGC 4490, NGC 4826 and NGC 5194 (clockwise from top left) (Sample 1). SFRSDs estimated using 1.4 GHz radio and FUV+24 μm emission are shown in contours and colors, respectively. Contour levels are listed below each panel of the figure. The circle in the bottom-left corner of the images indicates the angular resolution of the maps.

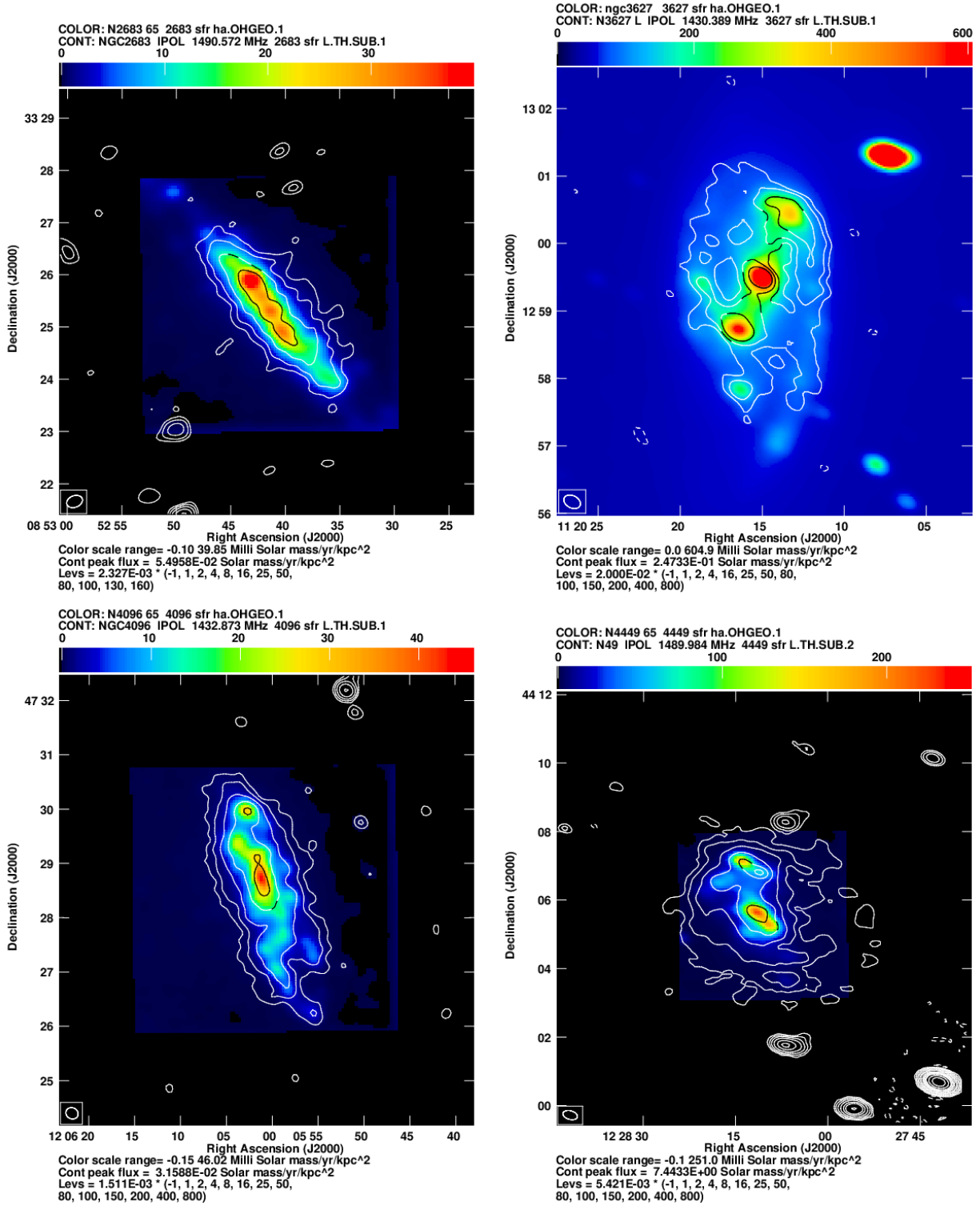


Figure 10. SFRSD ($M_{\odot}\text{yr}^{-1}\text{kpc}^{-2}$) maps of NGC 2683, NGC 3627, NGC 4449 and NGC 4096 (clockwise from top left) (Sample 1). SFRSDs estimated using 1.4 GHz radio and $H\alpha+24\mu\text{m}$ emission are shown in contours and colors, respectively. Contour levels are listed below each panel of the figure. The circle in the bottom-left corner of the images indicates the angular resolution of the maps.

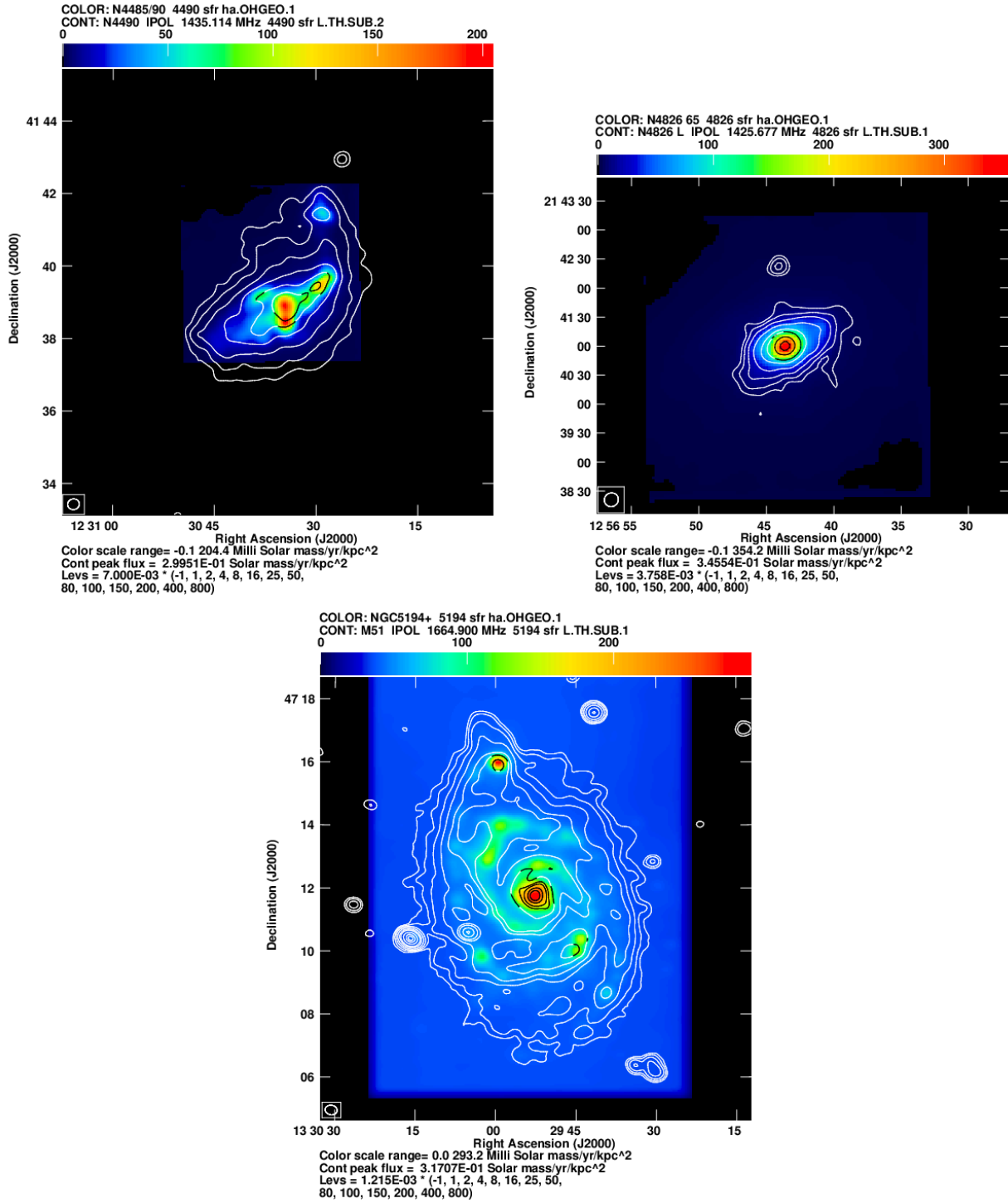


Figure 11. SFRSD ($M_{\odot}\text{yr}^{-1}\text{kpc}^{-2}$) maps of NGC 4490, NGC 4826 and NGC 5194 (clockwise from top left) (Sample 1). SFRSDs estimated using 1.4 GHz radio and $\text{H}\alpha+24\mu\text{m}$ emission are shown in contours and colors, respectively. Contour levels are listed below each panel of the figure. The circle in the bottom-left corner of the images indicates the angular resolution of the maps.